# ALL OPTICAL LOGIC GATES USING PLASMONIC RING RESONTORS

A

MAJOR PROJECT REPORT

MASTER OF TECHNOLOGY

IN

**VLSI DESIGN AND EMBEDDED SYSTEMS**

Submitted by:

**SREELEKSHMI R NAIR**

**2K19/VLS/19**

Under the supervision of

**Dr. YASHNA SHARMA**


**DEPARTMENT OF ELECTRONICS AND COMMUNICATION ENGINEERING**
DELHI TECHNOLOGICAL UNIVERSITY
(Formerly Delhi College of Engineering) Delhi-110042

**JANUARY 2021**

**DEPARTMENT OF ELECTRONICS AND COMMUNICATION ENGINEERING**
DELHI TECHNOLOGICAL UNIVERSITY
(Formerly Delhi College of Engineering) Delhi-110042

# CANDIDATE'S DECLARATION

I **Sreelekshmi R Nair** student of MTech (VLSI and Embedded Systems), hereby declare that the project Dissertation titled **"ALL OPTICAL LOGIC GATES USING PLASMONIC RING RESONTORS"** which is submitted by me to the Department of Electronics and Communication Engineering, Delhi Technological University, for Major Project-1, is original and not copied from any source without proper citation. This work has not previously formed the basis for the award of any Degree, Diploma Associateship, Fellowship or other similar title or recognition.

Place: Kochi **SREELEKSHMI R NAIR**

Date: 24-01-2020 (2K19/VLS/19)

**DEPARTMENT OF ELECTRONICS AND COMMUNICATION ENGINEERING**
DELHI TECHNOLOGICAL UNIVERSITY
(Formerly Delhi College of Engineering),Delhi-110042

# CERTIFICATE

I hereby certify that the Project Report titled **"ALL OPTICAL LOGIC GATES USING PLASMONIC RING RESONTORS"** which is submitted by **SREELEKSHMI R NAIR**, **2K19/VLS/19** of Electronics and Communication Department, Delhi Technological University, Delhi for the Major Project-1, is a record of the project work carried out by the student under my supervision. To the best of my knowledge this work has not been submitted in part or full for any Degree or Diploma to this University or elsewhere.

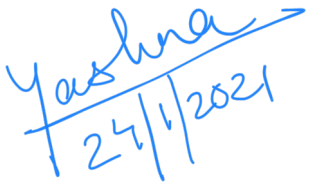


Place: Delhi
Date:

**Dr. YASHNA SHARMA**
**SUPERVISOR**

# ACKNOWLEDGEMENT

A successful project can never be prepared by the efforts of the person to whom the project is assigned, but it also demands the help and guardianship of people who helped in completion of the project. I would like to thank all those people who have helped me in this research and inspired me during my study.

With profound sense of gratitude, I thank Dr Yashna Sharma, my Research Supervisor, for her encouragement, support, patience and guidance in this project work. Furthermore, I thank Delhi Technological University for the support extended, especially to the Head of the Department and to the coordinator of MTech VLSI. I would also like to thank Nanophotonics and Plasmonics Lab (NPPL) at IIT Delhi for their support and resources.

I take immense delight in extending my acknowledgement to my family and friends who have helped me throughout this project work.

**SREELEKSHMI R NAIR**

Roll no: 2K19/VLS/19

# ABSTRACT

Electronic integrated circuit scaling, predicted by Moore, has been the driving force of the developments in semiconductor industry. But in the recent years, the rate predicted by Moore's law has deteriorated but the ever-increasing demand for energy-efficient and high-performance computing is still on the rise. Novel structures of transistors have already been developed to sustain the rate dictated by Moore's law. The current issues in the state-of-the-art CMOS technology are the interconnect bottleneck and heat management, which can be solved to an extent by employing light in the bottom layers of the circuit. To enable this, optical waveguides and devices must be scaled beyond the diffraction limit of light and it is enabled by plasmonics which provide subwavelength-scale confinement of light.

In plasmonics, surface plasmon polaritons (SPPs) is a key area for wave computing applications. SPPs are electromagnetic waves coupled to electron oscillations, supported by a metal-dielectric interface. The dispersion relation for SPPs yields the subwavelength-scale confinement. The electric field amplitude of the SPP wave decays exponentially perpendicular to the direction of propagation i.e, Transverse Magnetic mode is supported. This decay depends on the material in which the SPP wave resides and this results in a tradeoff between propagation length and confinement. So different waveguide topologies are suited for specific applications.

This works shows the theoretical details of surface plasmon polaritons and micro ring resonators in the point od view of employing them to realize all optical logic computing. A basic SOI ring resonator is implemented using 3-D FDTD in Lumerical FDTD Solver and various fields, on and off resonance were plotted. Further a Silver-Air-Silver Metal-Insulator-Metal waveguide is used to design an all optical NOT logic and various fields were observed using 2-D FDTD when input is enabled and disabled. Perfectly Matched Boundary Conditions were applied in both cases.

# TABLE OF CONTENTS


| | |
|---|---|
| **CANDIDATE'S DECLARATION** | ii |
| **CERTIFICATE** | iii |
| **ACKNOWLEDGEMENT** | iv |
| **ABSTRACT** | v |
| **TABLE OF CONTENTS** | vi |
| **LIST OF FIGURES** | vii |
| **LIST OF TABLES** | viii |
| **CHAPTER 1 INTRODUCTION** | 1 |
| 1.1 MOTIVATION | 2 |
| 1.2 ORGANIZATION OF THE REPORT | 2 |
| **CHAPTER 2 LITERATURE SURVEY** | 3 |
| **CHAPTER 3 ELECTROMAGNETICS IN METALS AND ON METAL SURFACES** | 5 |
| 3.1 MAXWELL'S EQUATION | 5 |
| 3.2 BULK PLASMONS OR VOLUME PLASMONS | 6 |
| 3.3 SURFACE PLASMON POLARITONS AT METAL/INSULATOR INTERFACES | 8 |
| 3.4 MULTILAYER SYSTEMS | 11 |
| **CHAPTER 4 MICRORING RESONATORS** | 13 |
| 4.1 PROPERTIES OF RING RESONATORS | 13 |
| 4.1.1 ALL PASS RING RESOANTOR | 13 |
| 4.1.2 ADD-DROP RING RESONATOR | 15 |
| 4.1.3 SPECTRAL CHARACTERISTICS | 15 |
| **CHAPTER 5 FINITE DIFFERENCE TIME DOMAIN (FDTD)** | 17 |
| 5.1 YEE'S ALGORITHM | 17 |
| 5.2 2-D YEE'S ALGORITHM | 18 |
| 5.3 TRANSVERSE MAGNETIC MODE | 19 |
| 5.4 ABSORBING BOUNDARY CONDITION | 20 |
| **CHAPTER 6 SIMULATION** | 22 |
| 6.1 SOFTWARE USED | 22 |
| 6.1.1 FDTD WORKFLOW | 22 |
| 6.2 SIMUALTION AND ANALYSIS OF A BASIC RING RESONATOR STRUCTURE | 22 |
| 6.2.1 SIMULATION SETUP AND RESULTS | 23 |
| 6.3 SIMULATION OF ALL OPTICAL PLASMONIC NOT GATE | 25 |
| 6.3.1 SIMULATION SETUP AND RESULTS | 26 |
| **CHAPTER 7 CONCLUSION AND FUTURE SCOPE** | 30 |
| **REFERENCES** | 31 |

# LIST OF FIGURES

***Figure 1. 1*** Current challenge presented by all optical logic gates.
***Figure 3. 1*** *The dispersion relation of the free electron gas. Electromagnetic wave propagation is only allowed for ω>ωp*
***Figure 3. 2*** *Longitudinal collective oscillations of the conduction electrons of a metal: Volume plasmons*
***Figure 3. 3*** *Geometry for SPP propagation at a single interface between a metal and a dielectric*
***Figure 3. 4*** *Decay of the $E_z$-field*
***Figure 3.5*** *Dispersion relation of a SPP at a single interface between semi-infinite gold and air sections with the real part (continuous line) and imaginary part (dashed line) separately plotted.*
***Figure 3.6*** *a: Schematic of a surface plasmon polariton b: Exponential decay of the electric field Ez perpendicular to the propagation direction. δm and δd indicate the decay length into the metal and dielectric respectively*
***Figure 3. 7*** *a) SPP at the multilayer MIM Interface b) Even and odd modes*
***Figure 4. 1*** *Geometry of a ring resonator*
***Figure 4. 2*** *(a)All pass ring resonator (b) its spectral response*
***Figure 4. 3*** *(a) An add-drop ring resonator (b) Spectral response*
***Figure 4. 4*** *Spectral parameters of a ring resonator*
***Figure 5. 1*** *Electric and magnetic field components in a 3D staggered cubic unit cell of the Yee space lattice.*
***Figure 5. 2*** *A 2D FDTD unit cell for transverse magnetic (TM) waves*
***Figure 5. 3*** *: (a) Schematic of a typical wave-equation problem, in which there is some finite region of interest where sources, inhomogeneous media, nonlinearities, etcetera are being investigated, from which some radiative waves escape to infinity. (b) The same problem, where space has been truncated to some computational region. An absorbing layer is placed adjacent to the edges of the computational region—a perfect absorbing layer would absorb outgoing waves without reflections from the edge of the absorber.*
***Figure 6. 1*** *Simulation Setup for SOI Ring Resonator*
**Figure 6. 2** Perspective view of the structure along with solver
***Figure 6. 3*** *Electric field distribution during On resonance condition (*$\boldsymbol{\lambda = 1.5328\mu m}$*)*
***Figure 6. 4*** *Electric field distribution at Off resonance condition(*$\boldsymbol{\lambda = 1.5\mu m}$*)*
***Figure 6. 5*** *Transmission Spectra at all four ports*
***Figure 6. 6*** *Transmission spectra at the through port*
***Figure 6. 7*** *Variation of S parameters when the ring radius is swept from 2.9 µm to 3.2µm*
***Figure 6. 8*** *Simulation setup for All-optical plasmonic NOT gate*
***Figure 6. 9*** *Perspective view of the structure along with solvers*
***Figure 6. 10*** *Refractive index profile of the structure*
***Figure 6. 11*** *Electric field distribution when input source is disabled*
***Figure 6. 12*** *Magnetic field distribution when input source is disabled*
***Figure 6. 13*** *Power distribution when input source is disabled*
**Figure 6. 14** Electric field distribution when input source is enabled
**Figure 6. 15** Magnetic field distribution when input source is disabled
***Figure 6. 16*** *Power distribution when input source is disabled*
***Figure 6. 17*** *Transmission Spectrum at Output port when input is disabled*
***Figure 6. 18*** *Transmission Spectrum at Output port when input is enabled*

# LIST OF TABLES

*Table 1 :Structural specifications of SOI ring resonator*
*Table 2 :Structural specifications of All optical plasmonic NOT gate*

# CHAPTER 1

# INTRODUCTION

Today's state-of-the-art microprocessors use fast transistors with dimensions on the order of 14 nm. But there lies a significant drawback when it comes to transferring digital information to the other end of a microprocessor that may be even a few centimeters away. Even though the conversion of the IC fabrication industry from aluminum to copper interconnects helped in an improvement of resistivity and electromigration for a brief period, it did not resolve the degradation of interconnect delay with further scaling down of feature sizes. Furthermore, numerous other issues still remain with metal interconnects including high power consumption, heating problem and Electromagnetic Interference (EMI). These limitations has become more evident over the recent years, as the rate of increase in the clock speed of microprocessors slowed down.

Although fiber optic interconnect cables can transfer digital data with a capacity >1000 times that of electronic interconnects they are around 1000 times larger compared with electronic components. A circuit with nanoscale features that can carry optical signals and electric currents would be the ideal solution to these issues. One such solution is the is the surface plasmons, which are electromagnetic waves that propagate along the surface of a conductor. Plasmonics concerns to the study of interaction of light with matter and subsequent electron oscillations in metallic nanostructures and nanoparticles. Plasmonic circuits possess the ability to carry optical signals and electric currents through the same thin metal circuitry, thereby creating the platform to combine the superior technical advantages of photonics and electronics on the same chip.The integration of optics and electronics is limited by their incomparable sizes. Electronic circuits can be fabricated at dimensions below 100 nm. On the contrary, the wavelength of light used in photonics circuits is in the order of 1000 nm. When the dimensions of optical components become comparable with wavelength of light, diffraction obstructs the propagation of light thereby hindering the scaling of optical components. Photonic crystals provided a partial solution to this problem. A more promising solution is plasmonics - the study concerning surface plasmons, since it encompasses both the capacity of photonics and miniaturization of electronics.

Surface plasmon allows to confine light to very small dimensions. SPs are light waves that occur at a metal/dielectric interface, where a group of coherent electrons collectively oscillates. These waves are trapped near the surface as they interact with the plasma of electrons near the surface of the metal. The resonant interaction between electron-charged oscillations near the surface of the metal and the electromagnetic field of the light creates the SP and thus it is a quasi-particle. SPs are bound to the metallic surface with exponentially decaying fields in both neighboring media. The decay length of SPs into the metal is defined by the skin depth, which is of the order of 10 nm—two orders of magnitude smaller than the wavelength of the light in air. This enhances the possibility of localization and the guiding of light in subwavelength metallic structures, and it can be used to construct miniaturized optoelectronic circuits with subwavelength components like waveguides, switches, couplers, modulators, resonators etc. Besides the excellent mode confinement, plasmonic devices have another significant advantage: the strong enhancement of the electromagnetic field. It is followed by many special physical properties, such as optical gradient forces, surface enhanced roman scattering (SERS) which are widely applied in optical trapping, nonlinear optics, etc. [1].

## 1.1 MOTIVATION

When in it comes to transmission and processing of data at high speeds, data are generally encoded on photons for transmission, which is then converted to the electronic signals for the faster processing. This is due to the fact that electrons can strongly interact with each other even in vacuum, while photon–photon interactions require the presence of a suitable medium to for such an interaction. For this reason, electronic systems are used for signal processing and Boolean operations. On the contrary, optical carriers (with a frequency generally between 150 and 3000 THz) are used to transmit data over large distances, at a very high bit rate, and without the need of any regeneration stage. The need for ultrafast and mass-producible components for telecommunication and sensing applications, calls for the ability of optical components to manipulate signals. Integrated photonic platforms have rapidly developed, allowing scientists to realize the basic set of functionalities needed in a standard optical network, namely signal switching, routing, wavelength and format conversion, phase conjugation, phase sensitive amplification, time-lens based optical Fourier transformation and signal regeneration. All optical flip-flops and logic gate are under study with the aim of implementing faster speed and lower energy consumption by replacing electrical circuits with photonic circuits. More specifically, they could be used in optical routers where signals are transmitted with light.

The current state -of-art in all optical logic fac a lot of challenges and trade-offs. One of the reasons for considering all optical logic is the power saving due to the elimination of electro-optic conversion, but this improvement would we significant only id the system is fast enough. Another challenge faced is the difficulty in mass production and uniformity of structural parameters which is crucial. Another major challenge is the scalability. To ensure scalability, the input and output ports must be identical, the output power of a gate should be good enough to drive other gates in cascade and the system must be robust in case of power supply fluctuations [2].

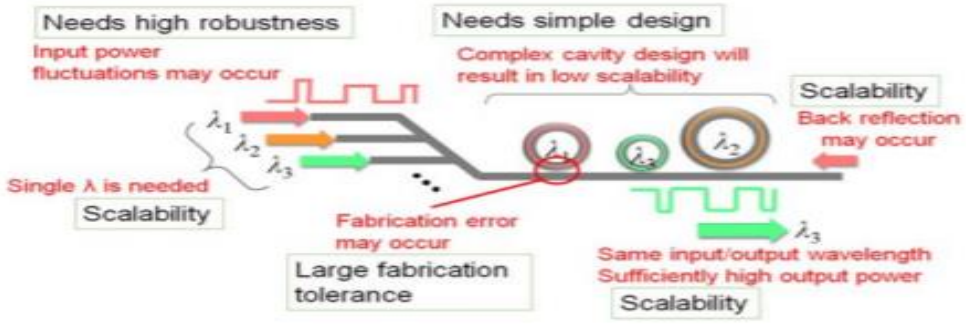


*Figure 1. 1 Current challenges presented by all optical logic gates.*

## 1.2 ORGANIZATION OF THE REPORT

This report comprises of 6 chapters. Chapter 1 discusses the background of Plasmonics. The literatures that deal with all optical logic gates are briefly discussed in chapter 2. Chapter 3 deals with the theoretical details of Surface Plasmon Polaritons. Chapter 4 gives a brief overview of ring resonator structure and its performance factors. Chapter 5 introduces the method called FDTD, used for solving Maxwell's equations in a plasmonic structures.

# CHAPTER 2

# LITERATURE SURVEY

Several studies have been proposed and investigated on the topic All-optical logic gates. Few of them are discussed here.

Almeida et al. proposed the use of resonant structures with high confinement and more sensitivity of transmission response on change in refractive index. Experimental results of an all-optical gate based on a silicon micrometer-size planar ring resonator, which operates with low pump-pulse energies were presented. A strong modulation of transmitted signal was achieved by varying the resonant frequency brought about by the tuning of refractive index. Further minimization was limited by the decrease in wavelength selectivity and eventually the Q factor but the speed was far better than the then available switches [3]

S. Kaur and R. S. Kaler proposed a gate structure that could implement AND, OR and NOT reconfigurable logic by employing only a single Semiconductor Optical Amplifier. The above logic was implemented at 40 Gb/s using Return to Zero modulated signals. Adequate values of extinction and contrast ratios were obtained and also the structure is suitable for photonic integration as it is compatible with CMOS technology [4].

A plasmonic component coupled to a silicon-on-insulator photonic crystal nanobeam cavity was proposed by Ivan S. Maksymov. It had the advantage that it exhibited the combined characteristics of a photonic cavity and plasmonic element, and also exploited the properties of Fano resonances resulting from interactions between the continuum and the localized cavity states. The probe signal could be controlled by a strong cavity mode damping offered by plasmonic element thereby enabling the implementation of logic gates and switches [5].

A structure composed of a silicon micro-ring resonator coupled to a straight waveguide fabricated on SOI substrate using E-beam lithography, plasma dry etching, and plasma enhanced chemical vapor deposition (PECVD) for the SiO2 cladding deposition was studied by Q. Xu and M. Lispon. The logic operation was implemented based on the proposal in [3]. A strong optical control pulse and a weak continuous wave probe light are coupled into the ring resonator. Free carriers in the ring resonator are generated by the control pulse by virtue of due to the two-photon absorption (TPA) effect. These free carriers lower the refractive index of silicon through plasma dispersion effect and a blue-shift occurs in the resonant wavelength. This modulates the output power of the probe light. The resonant wavelength and the transmission of the probe light relax back due to the fast surface recombination of the free carriers once the control signal is removed. The extent of modulation and the strength of control pulse showed a dependency like logic gates. With the right choice of energy of control pulse, AND and NAND logic functionality were implemented [6].

AND, OR and NOT gates were implemented using silver nanowires with interconnections between them. Later these implementations were cascaded among them themselves to implement the functionalities of universal logic gates. The logical functionality was implemented by manipulation polarization and phase dependent interference between output beams [7].

A structure composed of plasmonic waveguides coupler with nano disk of the size of a few nanometers were proposed and analyzed for its behavior as logic gates. XOR, XNOR, NAND and NOT gates were realized and FDTD simulations reveal the dependence of performance on structural characteristics of the proposed geometry. More logic functionalities can be implemented by cascading and combining the above-mentioned realizations [8].

An MIM structure with symmetric ring resonators and straight waveguides were proposed and numerically investigate using FDTD method. By using the coupling between the straight waveguide and ring resonator and by exploiting the dependence of the radii of the rings on resonant frequency, a NOT gate was implemented. A control input was used to manipulate the transmission of input signal to the output port [9].

Fu et al. proposed the realization of XOR, XNOR, NOT and OR gates using plasmonic Au-$SiO_2$ slot waveguide structure by exploiting the linear interference between various surface plasmon polariton modes. A huge improvement in the miniaturization and intensity improvement was observed in this structure which was excited with a laser beam of 830nm and a high contrast ratio between logic 1 and logic 0 levels were obtained [10].

A T-shaped switch built using a square shaped ring resonator was employed as the basic building block for the realization of NOT, AND and NOR gates. Light intensity was controlled by non linear Kerr self and cross phase modulation. The subwavelength size and low input pumping power together with high contrast ratio between ON and OFF states makes it suitable for photonic integrated circuits [11].

All seven logic gates AND, OR, NOT, NAND, NOR, XOR and XNOR were implemented using a structure comprised of Insulator-Metal-Insulator straight waveguides and nanorings made of Silver-Teflon and was analyzed by solving Maxwell's equations using 2-D FEM method using a perfectly matched boundary condition. By examining the transmission characteristics, the transmission threshold was determined [12]. Similar behavior was implemented using Silver- Sapphire plasmonic waveguides [13].

# CHAPTER 3

# ELECTROMAGNETICS IN METALS AND ON METAL SURFACES

Plasmons and Photons are the fundamental excitations in a material exhibiting conducting properties such as metal or extremely doped semiconductors. The free electron model considers metals as a gas of free electrons that are allowed to move freely within them. These electrons participate in electrical conduction and move independently throughout the lattice without interacting with each other and with the ion cores. Thus, the free electrons form the metal plasma comprising of positively charged ions and negatively charged electrons. Due to the low mass of electrons, they possess higher kinetic energies than those of ions. As a result of which the coupled excitation of electrons i.e., plasmons completely dominate the collective excitations of ions i.e., phonons. Plasmon is a quantum of collective excitation of conduction electrons inside a conducting media. There are two types of plasmons namely, Volume plasmon and Surface plasmon. Volume plasmons or Bulk plasmons arise due to longitudinal oscillations of electrons in a bulk material, whereas Surface plasmon is described as a surface wave arising by virtue of oscillations of free electron density at conductor surface.

As is well known from everyday experience, for frequencies up to the visible part of the spectrum metals are highly reflective and do not allow electromagnetic waves to propagate through them. Metals are thus traditionally employed as cladding layers for the construction of waveguides and resonators for electromagnetic radiation at microwave and far-infrared frequencies. In this low-frequency regime, the perfect or good conductor approximation of infinite or fixed finite conductivity is valid for most purposes, since only a negligible fraction of the impinging electromagnetic waves penetrates into the metal. At higher frequencies towards the near-infrared and visible part of the spectrum, field penetration increases significantly, leading to increased dissipation, and prohibiting a simple size scaling of photonic devices that work well at low frequencies to this regime. Finally, at ultraviolet frequencies, metals acquire dielectric character and allow the propagation of electromagnetic waves, albeit with varying degrees of attenuation, depending on the details of the electronic band structure. Alkali metals such as sodium have an almost free-electron-like response and thus exhibit an ultraviolet transparency. For noble metals such as gold or silver on the other hand, transitions between electronic bands lead to strong absorption in this regime.

These dispersive properties can be described via a complex dielectric function $\varepsilon(\omega)$. The underlying physics behind this strong frequency dependence of the optical response is a change in the phase of the induced currents with respect to the driving field for frequencies approaching the reciprocal of the characteristic electron relaxation time $\tau$ of the metal.

Macroscopic Maxwell equations forms the basics of optical properties of metals and has advantage that details of the fundamental interactions between charged particles inside media and electromagnetic fields need not be taken into account, since the rapidly varying microscopic fields are averaged over distances much larger than the underlying microstructure.

## 3.1. MAXWELL'S EQUATIONS

The interaction of metals with electro-magnetic fields can be completely described within the frame of

classical Maxwell equations:

$$\nabla \cdot D = \rho \quad (3.1)$$
$$\nabla \cdot B = 0 \quad (3.2)$$
$$\nabla \times E = -\partial B/\partial t \quad (3.3)$$
$$\nabla \times H = J + \partial D/\partial t, \quad (3.4)$$

which connects the macroscopic fields (dielectric displacement D, electric field E, magnetic field H and magnetic induction B) with an external charge density ρ and current density J.

The four macroscopic fields are further linked via the polarization *P* and magnetization *M* by

$$D = \varepsilon 0E + P \quad (3.5)$$
$$H = \frac{1}{\mu 0}B - M, \quad (3.6)$$

In the limit of linear, isotropic and non-magnetic media, there are few additional the material dependent relations:

$$D = \varepsilon_0 \varepsilon E \quad (3,7)$$
$$B = \mu_0 H \quad (3.8)$$

with a frequency dependent dielectric constant: ε= ε(ω), which is in general a complex function, $\varepsilon = \varepsilon' + i\,\varepsilon''$. It is furthermore connected to the complex index of refraction via $n = n + i\kappa = \sqrt{\varepsilon}$. Explicitly one can obtain the following expressions:

$$\varepsilon' = n^2 + \kappa^2 \ , \ \varepsilon'' = 2\,n\,\kappa \quad (3.9)$$

$$n^2 = \frac{\varepsilon'}{2} + \frac{1}{2}\sqrt{\varepsilon'^2 - \varepsilon''^2} \quad (3.10)$$

The real part of the refractive index n(ω) is responsible for the dispersion in the medium, the imaginary part κ(ω) (extinction coefficient) determines the absorption. Beer's law describes the exponential decay of the intensity of a light beam (along the x direction) in a medium: $I(x) = I_0 \exp(-\alpha x)$. The absorption constant can then be determined from the extinction coefficient: $\alpha(\omega) = 2\kappa(\omega)\omega/c$.

## 3.2.BULK PLASMONS OR VOLUME PLASMONS

Over a wide frequency range, the optical properties of metals can be explained by a plasma model, where a gas of free electrons of number density n moves against a fixed background of positive ion cores. For alkali metals, this range extends up to the ultraviolet, while for noble metals interband transitions occur at visible frequencies, limiting the validity of this approach. In the plasma model, details of the lattice potential and electron-electron interactions are not taken into account. Instead, one simply assumes that some aspects of the band structure are incorporated into the effective optical mass m of each electron. The electrons oscillate in response to the applied electromagnetic field, and their motion is damped via collisions occurring with a characteristic collision frequency $\gamma = 1/\tau$. τ is known as the relaxation time of the free electron gas, which is typically on the order of 10−14 s at room temperature, corresponding to γ = 100 THz.
The equation of motion for an electron of the plasma sea subjected to an external electric field E, in this model is:

$$mx^{\cdot\cdot} + m\gamma\, x^{\cdot} = -Ee \qquad (3.11)$$

with the solution,

$$x(t) = e\, m(\omega 2 + i\gamma\omega)\, E(t) \qquad (3.12)$$

The electrons which are displaced relative to the atom cores then generate a polarization $P = -Nex$. From this it follows for the dielectric displacement and the dielectric constant (from Eq. 5)

$$D = \varepsilon_0\left(1 - \frac{\omega_p^2}{\omega^2 + i\gamma\omega}\right)E, \qquad (3.13)$$

where $\omega_p^2 = \frac{ne^2}{\varepsilon_0 m}$ is the plasma frequency of the free electron gas. Therefore, the dielectric function of the free electron gas is:

$$\varepsilon(\omega) = 1 - \frac{\omega_p^2}{\omega^2 + i\gamma\omega} \qquad (3.14)$$

The dielectric function of the free electron gas (Eq.14) is thus also known as the **Drude** model of the optical response of metals.

The real and imaginary components of this complex dielectric function $\varepsilon(\omega) = \varepsilon_1(\omega) + i\varepsilon_2(\omega)$ are given by :

$$\varepsilon_1(\omega) = 1 - \frac{\omega_p^2\tau^2}{1+\omega^2\tau^2} \qquad (3.15)$$

$$\varepsilon_2(\omega) = \frac{\omega_p^2\tau}{\omega(1+\omega^2\tau^2)} \qquad (3.16)$$

where we have used $\gamma = 1/\tau$.

The real part is related to a phase lag between the electric and magnetic fields and the imaginary part is related to energy absorption in the considered material. The permittivity derived here will be needed later on in the calculation of the dispersion relation and group velocity of SPPs.

In case low frequency regime, where $\omega\tau << 1$, metals are strongly absorbing. The absorption constant then is given by:

$$\alpha = \frac{2\omega_p^2\tau\omega}{c^2} \qquad (3.17)$$

The penetration depth of the fields at low frequencies on applying Beer's law becomes $\delta = 2/\alpha$ and is called the skin depth. However at large frequencies close to $\omega_p$, the approximation $\omega\tau >> 1$ is valid. In this case the damping term $i\omega\tau$ can be neglected and $\varepsilon(\omega)$ becomes approximately real:

$$\varepsilon(\omega) = 1 - \frac{\omega_p^2}{\omega^2} \qquad (3.18)$$

The dispersion relation of electro-magnetic fields can be determined from $k^2 = |k|^2 = \varepsilon\,\omega^2/c^2$:

$$\omega(k) = \sqrt{\omega_p^2 + \frac{k^2}{c^2}} \qquad (3.19)$$

This relation is plotted for a generic free electron metal in Fig. 3.1 For $\omega < \omega_p$, propagation of transverse electromagnetic waves is hindered but for $\omega > \omega_p$, the plasma supports transverse waves propagating with a group velocity $v_g = d\omega/dK < c$.

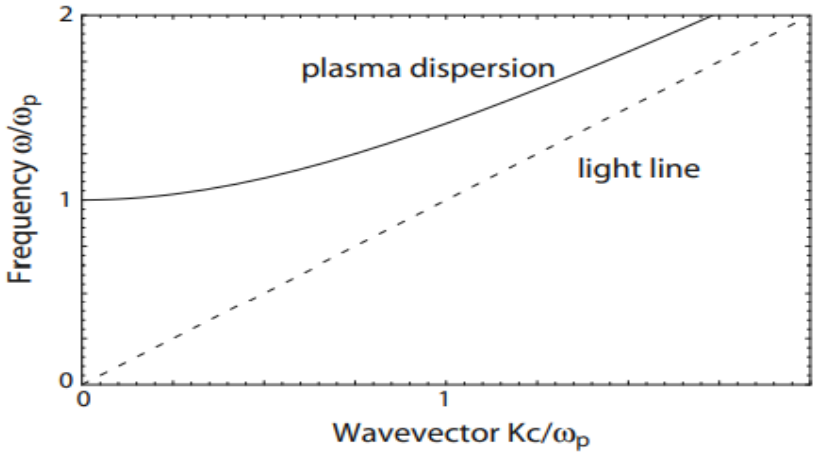


*Figure 3. 1 The dispersion relation of the free electron gas. Electromagnetic wave propagation is only allowed for ω>ωp*

In the small damping limit, $\varepsilon(\omega_p) = 0$ (for K = 0). This excitation must therefore correspond to a collective longitudinal mode as $\varepsilon(K, \omega_p) = 0$. The plasma frequency $\omega_p$ can thus be recognized as the natural frequency of a free oscillation of the electron sea. The quanta of these charge oscillations are called plasmons (or volume plasmons). Due to this longitudinal nature of the excitation, volume plasmons do not couple to transverse electromagnetic waves, and can only be excited by particle impact. Thus, the bulk plasma cannot be excited from or strayed to direct irradiation. Another consequence of this is that their decay occurs only via energy transfer to single electrons, a process known as Landau damping. In most metals, the plasma frequency is in the ultra-violet regime, with energies within 5-15 eV, depending on the metal band structure.

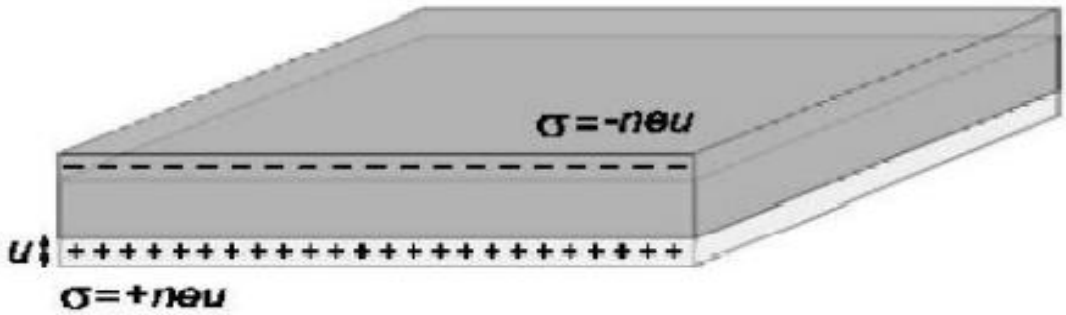


*Figure 3. 2 Longitudinal collective oscillations of the conduction electrons of a metal: Volume plasmons*

## 3.3.SURFACE PLASMON POLARITONS AT METAL / INSULATOR INTERFACES

Surface plasmon polaritons are electromagnetic excitations propagating at the interface between a dielectric and a conductor, evanescently confined in the perpendicular direction. These electromagnetic surface waves arise via the coupling of the electromagnetic fields to oscillations of the conductor's electron plasma.

Starting from Maxwell's equations, the system of equations governing TM modes are:

$$E_x = -i\frac{1}{\omega\varepsilon\varepsilon_0}\frac{\partial Hy}{\partial z} \quad (3.20)$$

$$E_z = -i\frac{\beta}{\omega\varepsilon\varepsilon_0}Hy \quad (3.21)$$

and the wave equation for TM modes is:

$$\frac{\partial^2 H}{\partial z^2} + (k_0{}^2\varepsilon - \beta^2)\,Hy = 0 \quad (3.22)$$

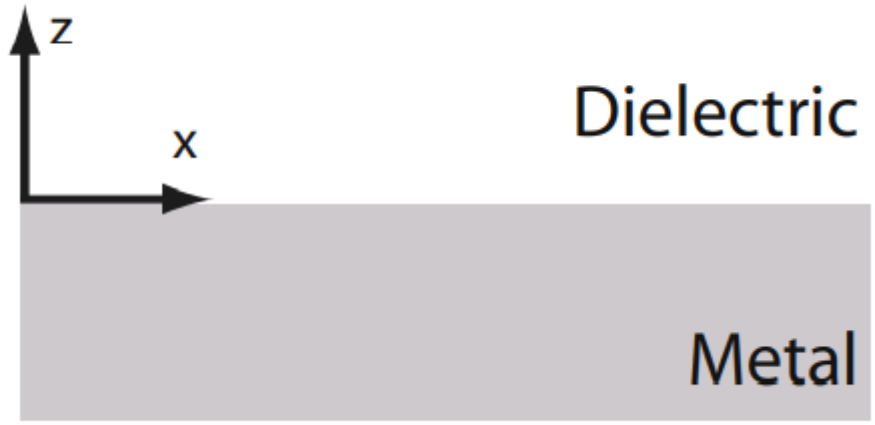


*Figure 3. 3 Geometry for SPP propagation at a single interface between a metal and a dielectric*

To detail the properties of SPPs, a one-dimensional problem of a single interface is considered here. The simplest geometry sustaining SPPs is that of a single, flat interface (Fig. 1.3) between a dielectric, non-absorbing half space ($z > 0$) with positive real dielectric constant $\varepsilon_2$ and an adjacent conducting half space ($z < 0$) described via a dielectric function $\varepsilon_1(\omega)$. The requirement of metallic character implies that Re $[\varepsilon_1] < 0$. As shown in section 1.2.2, for metals this condition is fulfilled at frequencies below the bulk plasmon frequency $\omega_p$. The propagating wave solutions confined to the interface, i.e. with evanescent decay in the perpendicular z-direction are discussed.

On applying the equations (20-22) in both half spaces we obtain:

$$E_Y(z) = A_2 e^{i\beta x} e^{-k_2 z} \quad (3.23)$$

$$H_X(z) = -iA_2\frac{1}{\omega\mu_0}k_2 e^{i\beta x} e^{-k_2 z} \quad (3.24)$$

$$H_z(z) = A_2\frac{\beta}{\omega\mu_0}e^{i\beta x} e^{-k_2 z} \quad (3.25)$$

For z>0 and

$$E_Y(z) = A_1 e^{i\beta x} e^{-k_1 z} \quad (3.26)$$

$$H_X(z) = -iA_1\frac{1}{\omega\mu_0}k_1 e^{i\beta x} e^{-k_1 z} \quad (3.27)$$

$$H_z(z) = A_1 \frac{\beta}{\omega\mu_0} e^{i\beta x} e^{-k_1 z} \qquad (3.28)$$

for z < 0.

The $E_z$-field is plotted both in the dielectric (z > 0) and metal (z < 0) in Figure 1.4 and this was realized by applying equations (23-25) and (26-28) at an air-gold interface and at a wavelength of 1550 nm. Notice the range of the y-axis differs by a factor of 50 between both plots, indicating the electric field decays much faster into the metal as compared with the electric field in the dielectric.

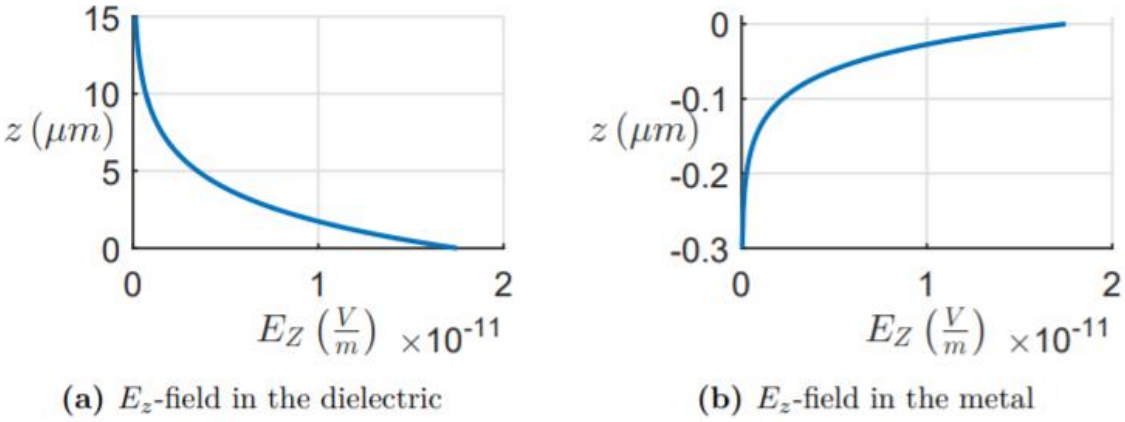


**(a)** $E_z$-field in the dielectric **(b)** $E_z$-field in the metal

*Figure 3. 4 Decay of the $E_z$-field*

Continuity of $E_y$ and $H_x$ at the interface leads to the condition

$$A_1 (k_1 + k_2) = 0 \qquad (3.29)$$

Since confinement to the surface requires Re [$k_1$] > 0 and Re [$k_2$] > 0, this condition is only fulfilled if $A_1 = 0$, so that also $A_2 = A_1 = 0$. Thus, no surface modes exist for TE polarization. Surface plasmon polaritons only exist for TM polarization. Also, continuity from Eqs. (23-25) and (26-29) between both the sections at z=0 implies that:

$$\frac{\varepsilon_2}{\varepsilon_1} = -\frac{k_{z,2}}{k_{z,1}} \qquad (3.30)$$

Using the relations (Eq. 23-30) dispersion relation of propagating surface plasmon polaritons (at a single metal-dielectric interface) can be obtained as:

$$\beta = \frac{\omega}{c}\sqrt{\frac{\varepsilon_2\varepsilon_1}{\varepsilon_2+\varepsilon_1}} \qquad (3.31)$$

Using the relative permittivity for air ($\varepsilon_2 = 1$) and assuming a metal is used without absorption losses is used, the dispersion relation can also be written as:

$$\beta = \frac{\omega}{c}\sqrt{\frac{\omega^2-\omega_p{}^2}{2\omega^2-\omega_p{}^2}} \qquad (3.32)$$

The different frequency regimes can be discussed from the plot of this relation.

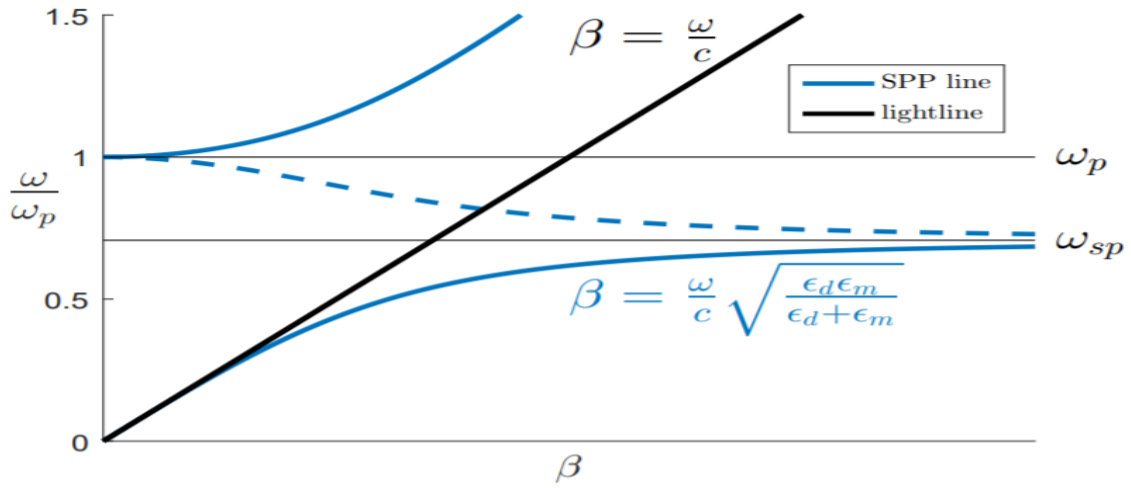


*Figure 3.5 Dispersion relation of a SPP at a single interface between semi-infinite gold and air sections with the real part (continuous line) and imaginary part (dashed line) separately plotted.*

The light line is the dispersion relation of a free photon. the real and imaginary components of the propagation constant are shown as a solid and dashed line respectively. In the low frequency regime($\omega_< \omega_p$), the SPP propagation constant, $\beta$ is comparable to $k_0$ and since $\beta$ is small, waves extend to the dielectric space over many wavelengths. . Radiation into the metal occurs in the transparency regime ($\omega > \omega p$). Between the regime of the bound and radiative modes, a frequency gap region with purely imaginary β, prohibiting propagation exists. The curve has an asymptote at the surface plasmon frequency $\omega_{sp}$ and at this frequency the group velocity $v_g = \frac{\partial \omega}{\partial k}$ becomes zero meaning the surface plasmon mode is static.

The surface plasmon frequency, $\omega_{sp}$ is given as

$$\omega_{sp} = \frac{\omega p}{\sqrt{1+\varepsilon_2}} \tag{3.33}$$

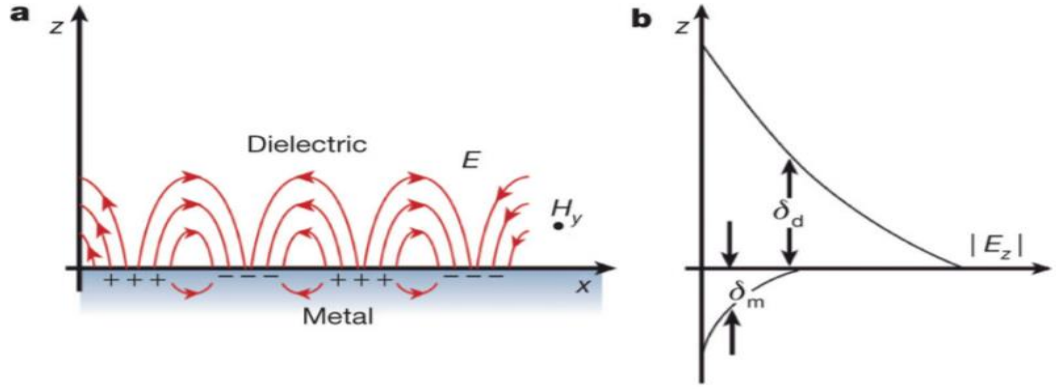


*Figure 3.6 a: Schematic of a surface plasmon polariton b: Exponential decay of the electric field Ez perpendicular to the propagation direction. δm and δd indicate the decay length into the metal and dielectric respectively*

## 3.4.MULTILAYER SYSTEMS

In multi-layer systems, each single interface can sustain bound SPPs. When the separation between adjacent interfaces is comparable to or smaller than the decay length of the interface mode, interactions between SPPs give rise to coupled modes. In order to elucidate the general properties of coupled SPPs we consider two types of systems- Metal-Insulator-Metal and Insulator-Metal-Insulator. On extending the dispersion relation in single interface systems to multilayer systems the following observations are

obtained.

In IMI geometry for odd modes, upon decreasing metal film thickness, the confinement of the coupled SPP to the metal film decreases as the mode evolves into a plane wave supported by the homogeneous dielectric environment. For real, absorptive metals described via a complex ε(ω), this implies a drastically increased SPP propagation length. The even modes exhibit the opposite behavior, their confinement to the metal increases with decreasing metal film thickness, resulting in a reduction in propagation length.

Whereas in MIM geometries, the fundamental odd mode of the system, does not exhibit a cut-off for vanishing core layer thickness. Thus, β does not go to infinity as the surface plasmon frequency is approached, but folds back and eventually crosses the light line, as for SPPs propagating at single interfaces. It is apparent that large propagation constants β can be achieved even for excitation well below $\omega_{sp}$, provided that the width of the dielectric core is chosen sufficiently small .

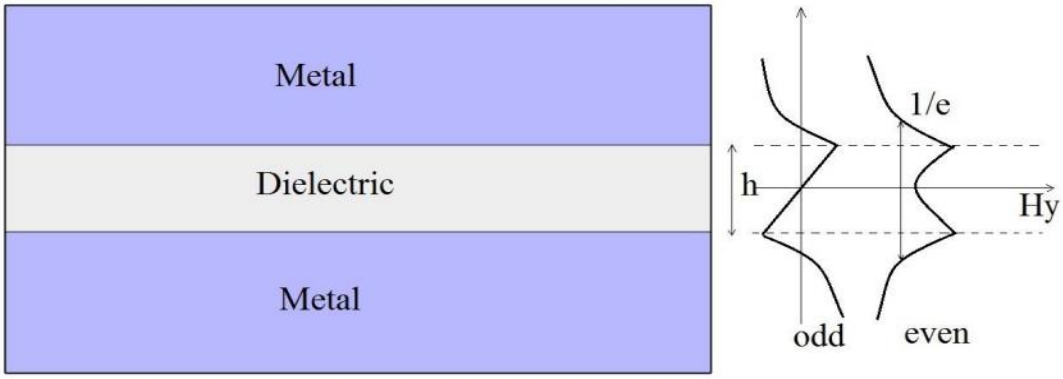


*Figure 3. 7 a) SPP at the multilayer MIM Interface b) Even and odd modes*

It is well known that the IMI waveguide exhibits less propagation loss, leading to longer propagation length than the MIM waveguide. On the other hand, from a point of confining light, since the skin depth of SPPs fields into the dielectric medium is much longer than that into the metallic medium at the interfaces , the MIM waveguide is better than the IMI waveguide. Thus, the MIM waveguide is more suitable for high optical integration [14].

# CHAPTER 4

# MICRORING RESONATORS

Optical ring resonators are waveguide structures that allow only a narrow band of frequency. They can also be used to couple two optical waveguides in opposite directions. A typical optical ring resonator has two parts, a straight waveguide, and a ring waveguide. The waveguide cores are placed close together and light waves are coupled from one waveguide to the other. In an optical ring resonator, light propagates around the loop and remains in the waveguides because of total internal reflection (TIR), a phenomenon in which light rays do not refract through the boundary of the medium they strike. Since only a few wavelengths reach resonance within these loops, optical ring resonators are used as filters. Two or more optical ring resonators can be combined to develop high-order optical filters with compact

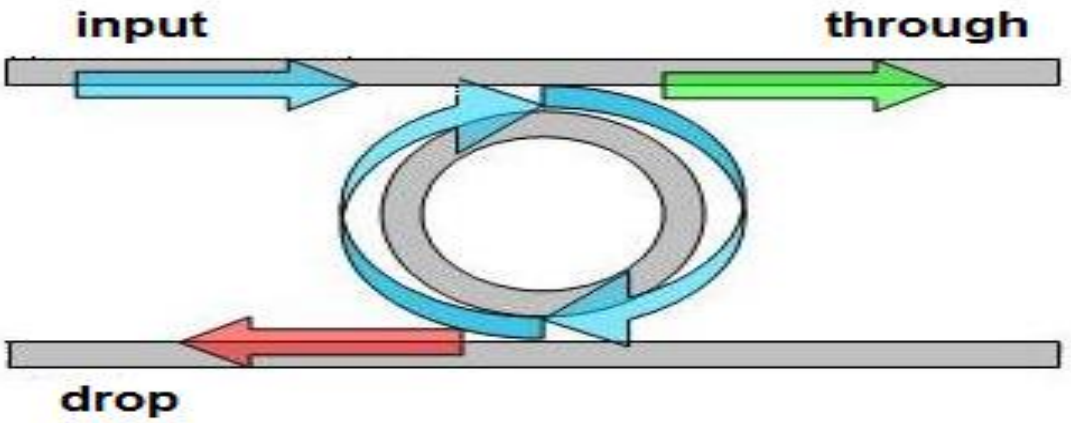


*Figure 4. 1 Geometry of a ring resonator*

size, minimal losses, and easy integration into existing networks.

## 4.1 PROPERTIES OF RING RESONATORS

In general, a ring resonator consists of a looped optical waveguide and a coupling mechanism to access the loop. When the waves in the ring build up a round trip phase shift that equals an integer times $2\pi$, the waves interfere constructively and the cavity is in resonance. Depending on the functionality, ring resonators are of two configurations:

- All pass ring resonators
- Add-drop ring resonators

### 4.1.1 ALL PASS RING RESONATOR

A basic all-pass ring resonator configuration can be thought of as looping one output of a directional coupler back to the input. In case the loop is elongated in the coupling region, it is called a racetrack resonator. The role of the waveguide is to couple light into the resonator. As it is shown in Figure 2.2, one input and one output port can be introduced for this filter. The

output port usually is named the through/pass port. The optical signal injected to the input port propagates through the waveguide to reach to the coupling region, which is the area of the waveguide with minimum distance with a ring resonator. In this region, a part of the light evanescently couples to the ring. The amount of coupling depends on the gap spacing between waveguide and ring, as well as matching between propagation constant of propagating mode through the waveguide and resonating mode inside the ring. The coupled light at resonance wavelengths, traps and builds up energy inside the ring. At other wavelengths, the light passes through the coupling region and reaches to the through port.

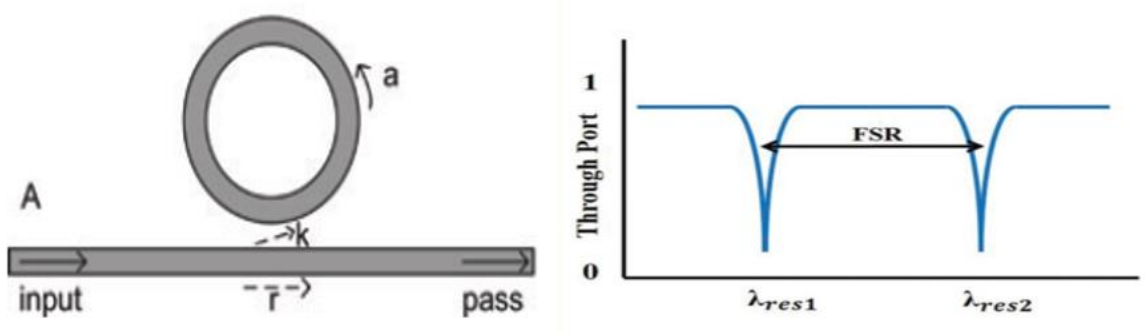


*Figure 4. 2 (a)All pass ring resonator (b) its spectral response*

Under the assumptions of continuous wave (CW) operation, matching fields and that the reflections back into the bus waveguide are negligible, the transfer function can be written as:

$$\frac{Epass}{Einput} = e^{i(\pi+\phi)} \frac{a - re^{-i\phi}}{1 - rae^{i\phi}} \quad (34)$$

$\phi = \beta L$ is the single-pass phase shift, with L the round-trip length and β the propagation constant of the circulating mode. a is the single-pass amplitude transmission, including both propagation loss in the ring and loss in the couplers. It relates to the power attenuation coefficient *α [1/cm]* as $a^2 = exp(-\alpha L)$.
By squaring Eq. (1), we obtain the intensity transmission Tn,

$$T_n = \frac{a^2 - 2racos\phi + r^2}{1 - 2arcos\phi + (ra)^2} \quad (35)$$

r is the self-coupling coefficient. Similarly, we can define k as the cross-coupling coefficients, so $r^2$ and $k^2$ are the power splitting ratios of the coupler, and they are assumed to satisfy $r^2 + k^2 = 1$, which means there are no losses in the coupling section. This assumption can introduce a small error on the transmission power levels.

The ring is said to be in resonance when the wavelength of light is an integral multiple of optical length,

$$\lambda_{res} = \frac{n_{eff}L}{m}, \text{ m=1,2,3…} \quad (36)$$

There are 3 cases of coupling between waveguide and ring based on the values of r and a:

- **Under coupling (r < a)**: The amount of light coupled into the cavity is insufficient to overcome the cavity loss and there is no phase build-up when light is on resonance.

- **Critical coupling (r = a)**: The amount of light coupled is equal to the cavity loss leading to zero transmission.
- **Over coupling (r > a)**: The amount of light coupled into the cavity is more than that lost inside it, resulting in a net phase build-up and a phase shift approximately equal to 2 $\pi$(a decrease in phase shift).

The phase argument of the field transmission varies periodically with frequency. All-pass resonators delay incoming signals via the temporary storage of optical energy within the resonator.

### 4.1.2 ADD-DROP RING RESONATOR

An add-drop structure includes two waveguides, which are placed on both sides of a ring resonator. The duty of one of the waveguides is to inject light to the resonator and the other one is responsible to couple light out of the resonator. As it is shown in Figure 4.2, four ports can be introduced for this structure. The optical resonance can be observed at two output ports. The first one at the other end of the input port is called the through/pass port. The transmission response of this port is similar to the through port of the all-pass filter, which means there is a dip at the transmission of the through port at resonance wavelength. The second output that has a reverse transmission response compared to through port is called drop port.

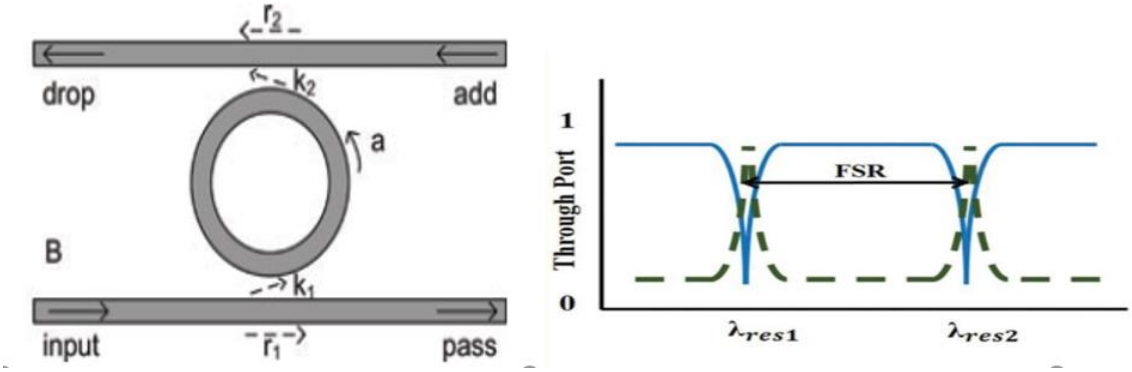


*Figure 4. 3 (a) An add-drop ring resonator (b) Spectral response*

The transmission to add and drop and drop port can be obtained as:

$$T_P = \frac{r_2 a^2 - 2r_1 r_2 a\cos\phi + {r_1}^2}{1 - 2r_1 r_2 a\cos\phi + (r_1 r_2 a)^2} \tag{37}$$

$$T_n = \frac{(1-r_1)^2(1-r_2)^2 a}{1 - 2r_1 r_2 a\cos\phi + (r_1 r_2 a)^2} \tag{38}$$

If the cavity loss coefficient, a =1, critical coupling occurs when $k_1 = k_2$.

### 4.1.3 SPECTRAL CHARACTERISTICS

The performance of resonators can be measured in terms of the free spectral range (FSR), the full width at half maximum (FWHM), the finesse, extinction ratio, and the quality factor. The full width at half maximum (FWHM) is a measure of the sharpness of the resonance. As the name suggests, it is given as the width of the resonance peak where the power drops to half of the resonance value. The free spectral range (FSR) is defined as the wavelength difference between two successive maxima of the dropped power (or minima of the through power).

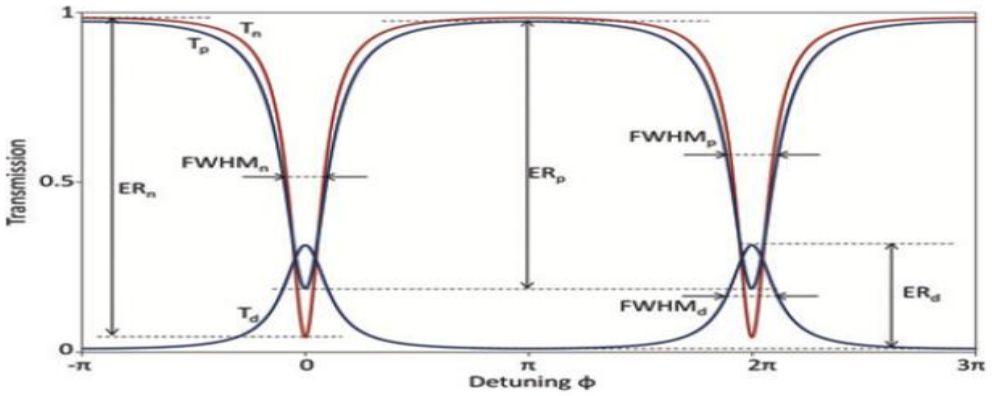


*Figure 4. 4 Spectral parameters of a ring resonator*

The finesse is defined as the ratio of FSR and resonance width and the Quality factor is the ratio of resonant wavelength to FWHM. It's a measure of the sharpness of resonance with respect to central frequency. Physically these terms can be explained in conjunction with the number of round trips of the cavity. The finesse is found to represent within a factor of 2π the number of round-trips made by light in the ring before its energy is reduced to 1/e of its initial value. The Q-factor represents the number of oscillations of the field before the circulating energy is depleted to 1/e of the initial energy. Another important parameter is the extinction ratio. It is the ratio of the amplitude of the signal in the through port at the resonant wavelength to that far away from the resonant wavelength in decibels [15].

# CHAPTER 5

# THE FINITE DIFFERNECE TIME DOMAIN (FDTD)

The Finite Difference Time Domain method (FDTD) is a powerful engineering tool for integrated and diffractive optics device simulations, mainly because of its unique combination of features, such as its ability to model light propagation, scattering and diffraction, and reflection and polarization effects. The FDTD method allows for the efficient and powerful simulation and analysis of submicron devices with very fine structural details. The FDTD method, which was first developed by Yee in 1966, is a numerical method for solving Maxwell's equations. Yee proposed a discrete solution to Maxwell's equations based on central difference approximations of the spatial and temporal derivatives of the two Maxwell's curl-equations.

## 5.1 YEE'S ALGORITHM

The algorithm used in FDTD simulations is known as the Yee algorithm. The original proposal was intended for homogeneous, isotropic and lossless media based on discretizing the volume into cells in Cartesian coordinates. The Yee algorithm solves for both electric and magnetic fields using the coupled Maxwell's time-dependent curl equations, rather than solving for the electric field alone (or the magnetic field alone) with a wave equation. In principle the Yee algorithm places all electric (E) and magnetic (M) fields in an interlinked array with respect to Faraday's and Ampere's Laws inside a cubic cell. The E and the H field components are interlaced in all three spatial dimensions as shown in Figure 5.1.

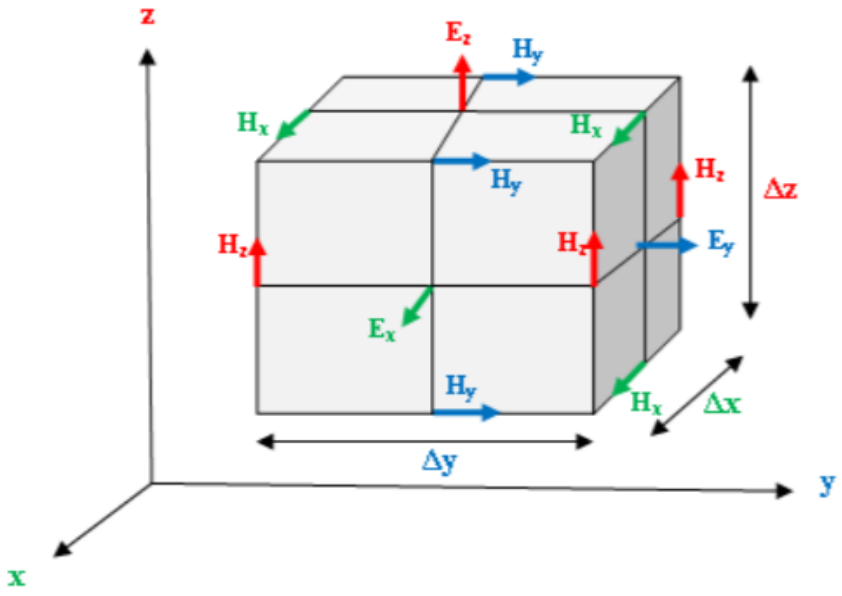


*Figure 5. 1 Electric and magnetic field components in a 3D staggered cubic unit cell of the Yee space lattice.*

This algorithm then solves both the E and H fields in a systematic approach: all of the E computations in the modelled space are completed and stored in computer memory for a particular time-point using previously stored H data. Then all the H computations in the space are completed using the E data just

computed. Inside a loop, this process continues until time-stepping, which is set by the user, is concluded. The computer simulation runtime increases with the size of the model and total number of time-steps.

The method starts with the Maxwell's equations (3.3) and (4.3) and results in six coupled scalar equations in a Cartesian coordinate that can be used to compute the field at a given mesh point.

$$\frac{\partial E_x}{\partial t} = \frac{1}{\varepsilon}\left(\frac{\partial H_z}{\partial y} - \frac{\partial H_y}{\partial z}\right) \quad (5.1)$$

$$\frac{\partial E_y}{\partial t} = \frac{1}{\varepsilon}\left(\frac{\partial H_x}{\partial z} - \frac{\partial H_z}{\partial x}\right) \quad (5.2)$$

$$\frac{\partial E_z}{\partial t} = \frac{1}{\varepsilon}\left(\frac{\partial H_y}{\partial x} - \frac{\partial H_x}{\partial y}\right) \quad (5.3)$$

$$\frac{\partial H_x}{\partial t} = \frac{1}{\mu}\left(\frac{\partial E_y}{\partial z} - \frac{\partial E_z}{\partial y}\right) \quad (5.4)$$

$$\frac{\partial H_y}{\partial t} = \frac{1}{\mu}\left(\frac{\partial E_z}{\partial x} - \frac{\partial E_x}{\partial z}\right) \quad (5.5)$$

$$\frac{\partial H_z}{\partial t} = \frac{1}{\mu}\left(\frac{\partial E_x}{\partial y} - \frac{\partial E_y}{\partial x}\right) \quad (5.6)$$

For simplicity, we will look at the discretization of these equations in the 2D cases and the same steps can be used for 3D cases.

## 5.2 2D YEE ALGORITHM

We will now look at discretization of Maxwell's equations based on the staggered cubic unit cell of the Yee space lattice given in Figure 5.1. In particular, we assume that there is no variation in the z direction. That means there is no propagation in the z direction, while propagation in either x- or y-directions (or both) is possible. Also, for simplicity, we neglect the magnetic or electric losses and assuming simple and source-free media, i.e., ε and μ are simple constants, independent of position, direction, or time. In the TM (TE) mode, only Hx and Hy (Ex and Ey) components are nonzero and are in the plane of propagation. We can now group Equation 4.1 according to field vector components. One set involving only Hx, Hy, and Ez, and another set involving Ex, Ey, and Hz, referred to respectively as the TM and TE modes. The resulting two sets of equations are given by :

$$\frac{\partial H_x}{\partial t} = -\frac{1}{\mu}\left(\frac{\partial E_z}{\partial y}\right) \quad (5.7)$$

$$\frac{\partial H_y}{\partial t} = \frac{1}{\mu}\left(\frac{\partial E_z}{\partial x}\right) \quad (5.8)$$

$$\frac{\partial E_z}{\partial t} = \frac{1}{\varepsilon}\left(\frac{\partial H_y}{\partial x} - \frac{\partial H_x}{\partial y}\right) \quad (5.9)$$

for TM mode.
Here we considering only the discretization of TM mode.

## 5.3 TRANSVERSE MAGNETIC (TM) MODE

A portion of the Yee cell constituting a unit cell for the TM case is depicted in Figure 5.2. Note the spatial positions of the two magnetic field components (Hx and Hy) and the electric field component (Ez). The Ez component is located at integer grid points (i, j); the Hx component is located at integer x and half y grid point and the Hy component is located at half x and integer y components.

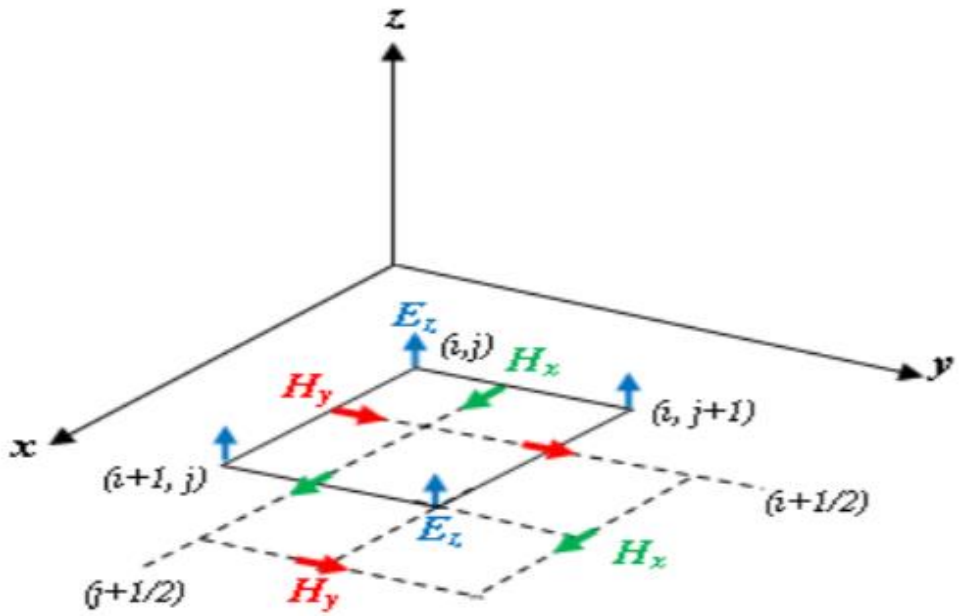


*Figure 5. 2 A 2D FDTD unit cell for transverse magnetic (TM) waves*

The spatially discretized versions of Equations 5.7-5.9 are:

$$\frac{\partial H_x}{\partial t}\Big|_{i,j+\frac{1}{2}} = -\frac{1}{\mu}\left[\frac{E_z|_{i,j+1} - E_z|_{i,j}}{\Delta y}\right] \qquad (5.10)$$

$$\frac{\partial H_y}{\partial t}\Big|_{i+\frac{1}{2},j} = \frac{1}{\mu}\left[\frac{E_z|_{i+1,j} - E_z|_{i,j}}{\Delta x}\right] \qquad (5.11)$$

$$\frac{\partial E_z}{\partial t}\Big|_{i,j} = \frac{1}{\varepsilon}\left[\frac{H_y|_{i+\frac{1}{2},j} - H_y|_{i-\frac{1}{2},j}}{\Delta x} - \frac{H_x|_{i,j+\frac{1}{2}} - H_x|_{i,j}}{\Delta y}\right] \qquad (5.12)$$

Solving Equations (5.10-5.12) for the time derivatives, the FDTD algorithm for TM waves is given by:

$$H_x\Big|_{i,j+\frac{1}{2}}^{n+\frac{1}{2}} = H_x\Big|_{i,j+\frac{1}{2}}^{n-\frac{1}{2}} - \frac{\Delta t}{u_{i,j+\frac{1}{2}}\Delta y}\left[E_z|_{i,j+1}^{n} - E_z|_{i,j}^{n}\right] \qquad (5.13)$$

$$H_x\big|_{i+\frac{1}{2},j}^{n+\frac{1}{2}} = H_y\big|_{i+\frac{1}{2},j}^{n-\frac{1}{2}} - \frac{\Delta t}{u_{i+\frac{1}{2},j}\Delta x}\left[E_z\big|_{i+1,j}^{n} - E_z\big|_{i,j}^{n}\right] \qquad (5.14)$$

$$E_z\big|_{i,j}^{n+1} = E_z\big|_{i,j}^{n} + \frac{\Delta t}{\varepsilon_{i,j}}\left[\frac{H_x\big|_{i+\frac{1}{2},j}^{n+\frac{1}{2}} - H_y\big|_{i-\frac{1}{2},j}^{n+\frac{1}{2}}}{\Delta x} - \frac{H_x\big|_{i,j+\frac{1}{2}}^{n+\frac{1}{2}} - H_x\big|_{i,j-\frac{1}{2}}^{n+\frac{1}{2}}}{\Delta x}\right] \qquad (5.15)$$

For the TM mode (Hx, Hy, Ez): $E \times H = -Ez\,Hy\,i - Ez\,Hx\,j$. So, the light intensity for the TM mode is given by[16]:

$$I = \langle \bar{S} \rangle_{TM} = \frac{1}{\mu_0}\bar{E} \times \bar{H} \qquad (5.16)$$

## 5.4 ABSORBING BOUNDARY CONDITION

One of the great advantages of the FDTD method is that it does not require the storage of any field more than one time step back. However, the necessarily finite nature of any FDTD spatial grid is a critical limitation in the FDTD method. This means that the problem at the boundaries of the FDTD grid arises because the field components at the outer edge of a finite FDTD space are not completely surrounded by the field components required for an updated equation. Accordingly, there is not enough information to correctly update these components during the implementation of the FDTD algorithm. An absorbing boundary condition (ABC) is a means of approximately estimating the missing field components just outside the FDTD grid, in order to emulate an "infinite" space. Such an approximation typically involves assuming that a plane wave is incident on the boundary and estimating the fields just outside the boundary by using the fields just inside the boundary. In general, different ABCs are better suited for different applications and the choice of a particular ABC is also made by considering its numerical efficiency and stability properties. Among the different types of absorbing boundary conditions, our interest is specific to those based on surrounding the FDTD domain with a layer of absorbing material, known as Perfectly Matched Layers (PML).

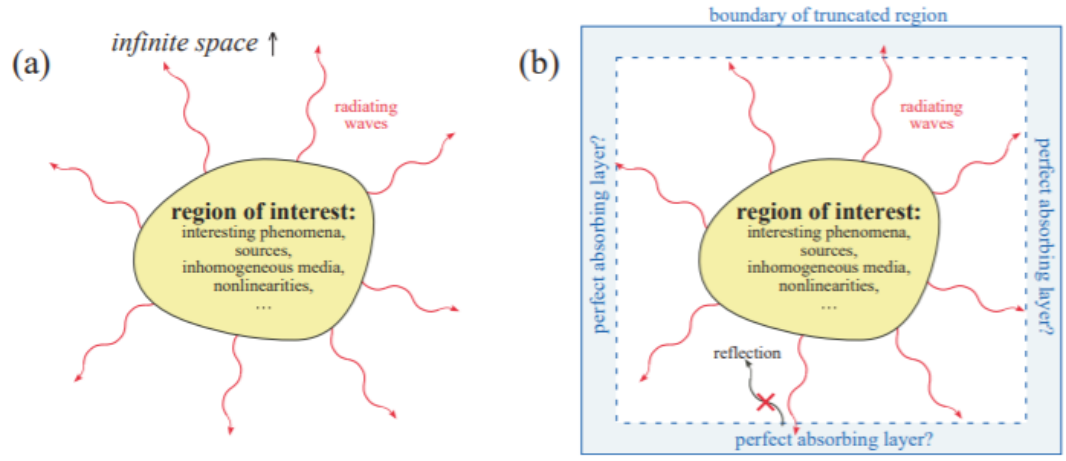


*Figure 5. 3 : (a) Schematic of a typical wave-equation problem, in which there is some finite region of interest where sources, inhomogeneous media, nonlinearities, etcetera are being investigated, from which some radiative waves escape to infinity. (b) The same problem, where space has been truncated to some computational region. An absorbing layer is placed adjacent to the edges of the computational region—a perfect absorbing layer would absorb outgoing waves without reflections from the edge of the absorber.*

A perfectly matched layer (PML) is an artificial absorbing medium that is commonly used to truncate computational grids for simulating Maxwell's equations, and is designed to ensure that interfaces between the PML and adjacent media are reflectionless. The first effective PML was introduced by J. P. Berenger in 1994. Berenger's PML method for absorbing waves which are incident on the boundaries of an FDTD grid is based on reflection and refraction of uniform plane waves at the interface between a lossless dielectric and a general lossy medium. The PML method involves modifying the medium of the simulation in a thin layer around the boundary, as shown in Figure 4.4, so that this layer becomes an artificially "absorbing" or lossy medium. The boundary layer is designed so that it absorbs enough of the outgoing wave so that reflections from the actual boundary are acceptably low. In addition, however, the boundary layer must be designed to prevent reflections from the interface between the actual medium and this boundary medium. This means the two media must be impedance-matched to very high accuracy. For this reason, the family of these methods is known as perfectly matched layers, or PMLs[17].

# CHAPTER 6

# SIMULATION

## 6.1 SOFTWARE USED

The tool used for the simulation and analysis of ring resonator and plasmonic logic gates here is Lumerical FDTD, which is a multipurpose designing tool for simulating and optimizing the performance of photonic integrated circuits. Lumerical FDTD solver uses the industry accepted FDTD method to accurately simulate the photonic and plasmonic devices involving subwavelength structures. It can solve arbitrary geometries and materials over any source bandwidth.

### 6.1.1 FDTD WORKFLOW

- Define Geometry
- Define simulation region and mesh details.
- Define the radiation source
- Add monitors and analysis tools
- Run simulation
- Visualize results
- Run parametric sweeps and optimizations

## 6.2 SIMUALTION AND ANALYSIS OF A BASIC RING RESONATOR STRUCTURE

A basic Silicon on Insulator (SOI) ring resonator structure is simulated in 3-D FDTD with the following structural specifications:

| **Substrate** | |
|---|---|
| Material | SiO2 (Glass)- Palik |
| Dimensions | $16\times 16 \times 4$ ($\mu m$) |
| **Ring Resonator** | |
| Material | Silicon-Palik |
| Radius | 3.1μm |
| Coupling gap | 0.1 μm |
| Base width of waveguide | 0.4 μm |
| Base height of waveguide | 0.18 μm |
| **Ports** | |
| Type | Mode Source |
| Wavelength start | 1.5μm |
| Wavelength start | 1.6μm |
| **Monitors** | Frequency domain field profile |
| **Boundary Condition** | PML |

*Table 1 :Structural specifications of SOI ring resonator*

### 6.2.1 SIMULATION SETUP AND RESULTS

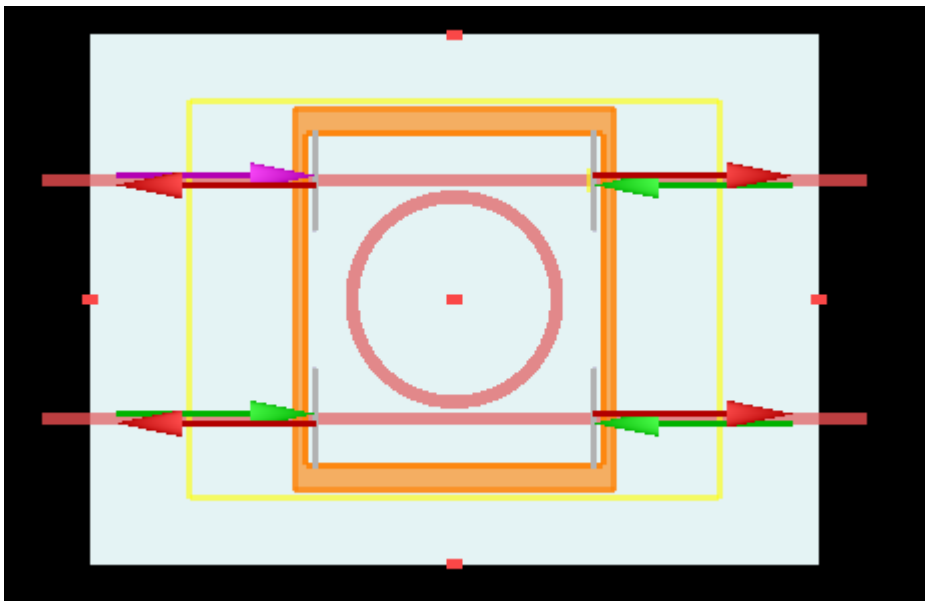

*Figure 6. 1 Simulation Setup for SOI Ring Resonator*

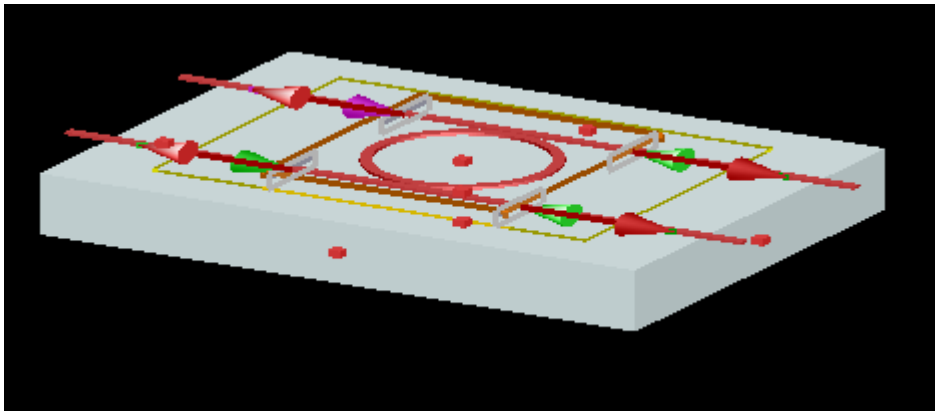

*Figure 6. 2 Perspective view of the structure along with solver*

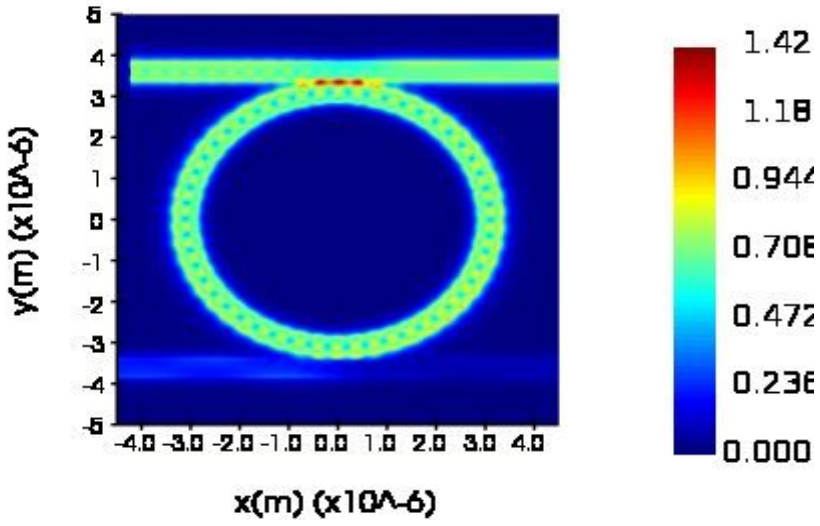


*Figure 6. 3 Electric field distribution during On resonance condition ($\boldsymbol{\lambda = 1.5328\mu m}$)*

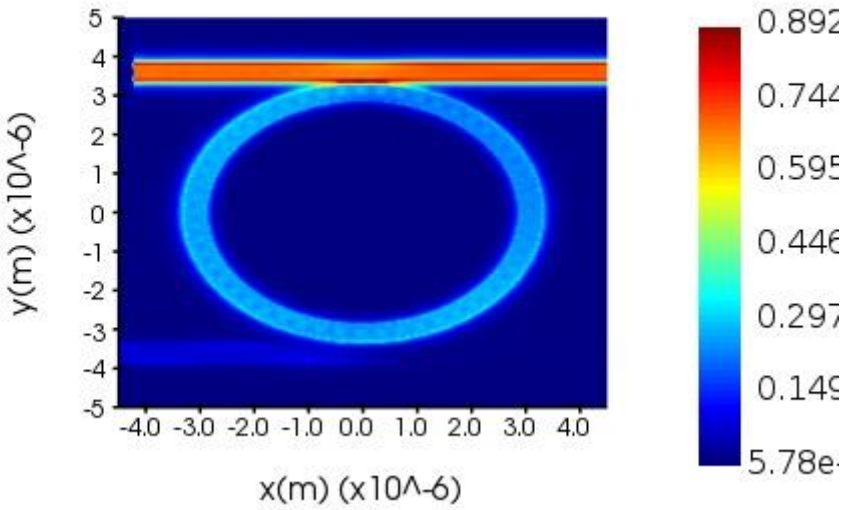


*Figure 6. 4 Electric field distribution at Off resonance condition($\boldsymbol{\lambda = 1.5\mu m}$)*

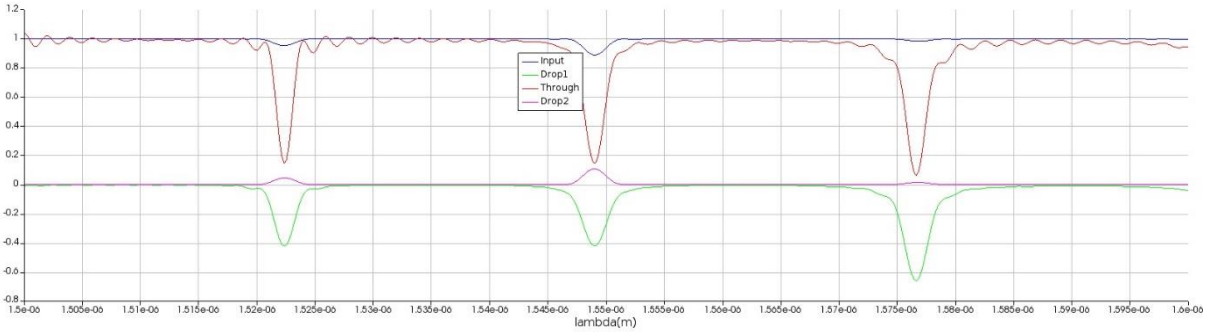


*Figure 6. 5 Transmission Spectra at all four ports*

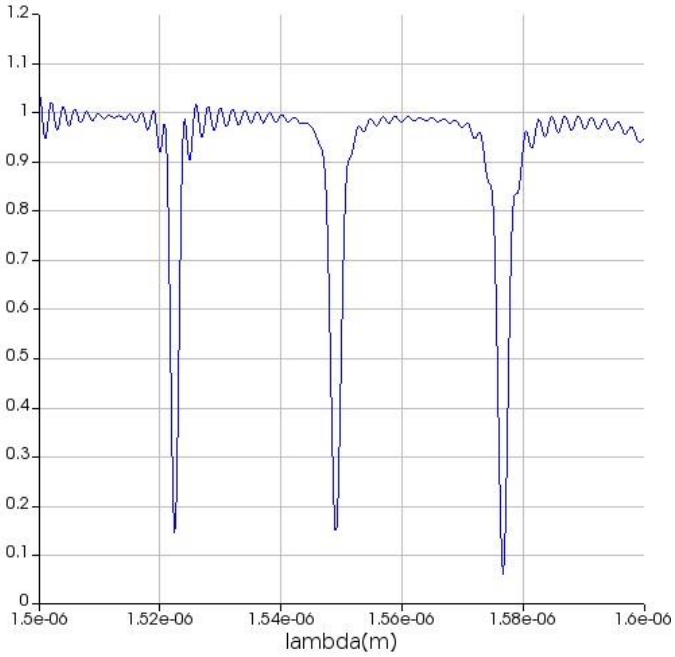


*Figure 6. 6 Transmission spectra at the through port*

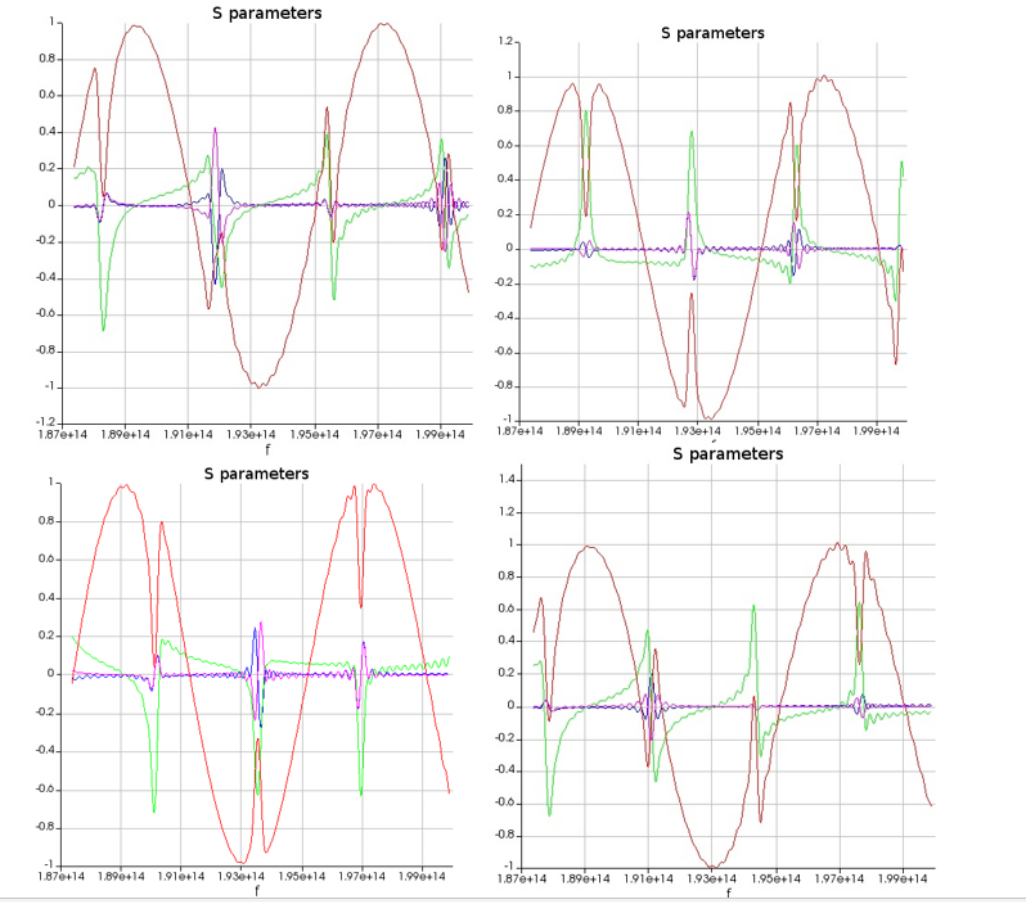


*Figure 6. 7 Variation of S parameters when the ring radius is swept from 2.9 µm to 3.2µm*

## 6.3 SIMULATION OF ALL-OPTICAL PLASMONIC NOT GATE

An all-optical plasmonic NOT logic using a Silver-Air-Silver MIM waveguide is simulated in 2-D FDTD method.

The structural specification of the setup is elaborated in the table below:

| **Substrate** | |
|---|---|
| Material | Ag (Silver)- Johnson and Christy |
| Dimensions | 1.6× 1.5 (µ$m$) |
| **Ring Resonator** | |
| Material | Air ($n$=1.0003) |
| Radius | 0.1µm |
| Coupling gap | 0.02 µm |
| Base width of ring | 0.05 µm |
| Base width of straight waveguide | 0.05 |
| **Ports** | |
| Type | Mode Source |
| Wavelength start | 0.61 µm |
| Wavelength start | 1.11 µm |
| **Monitors** | Frequency domain field profile |
| **Boundary Condition** | PML |

*Table 2 :Structural specifications of All optical plasmonic NOT gate*

### 6.3.1 SIMULATION SETUP AND RESULTS

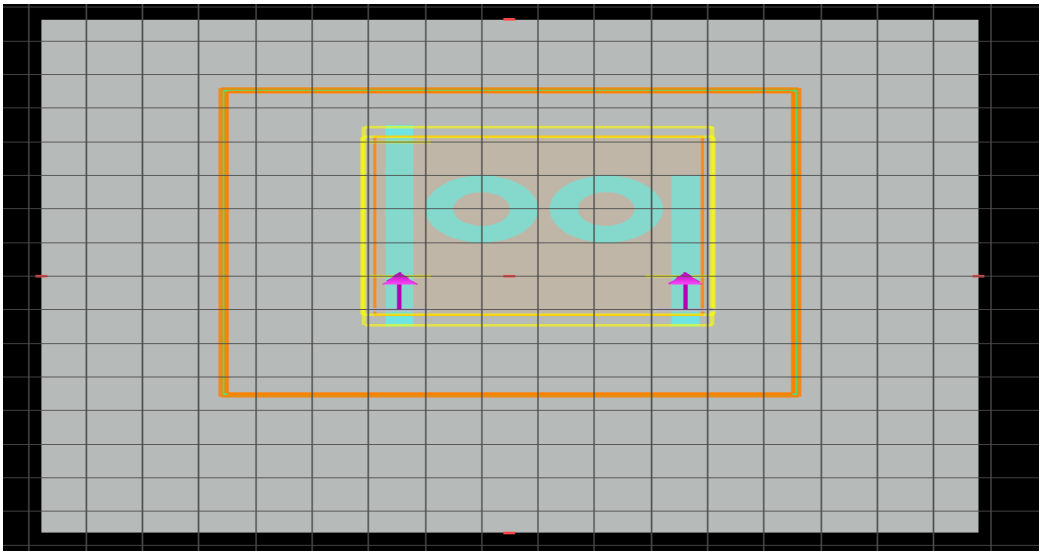

*Figure 6. 8 Simulation setup for All-optical plasmonic NOT gate*

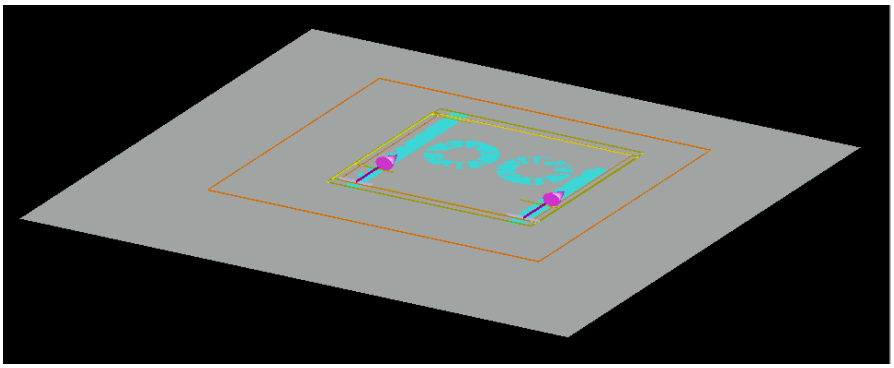

*Figure 6. 9 Perspective view of the structure along with solvers*

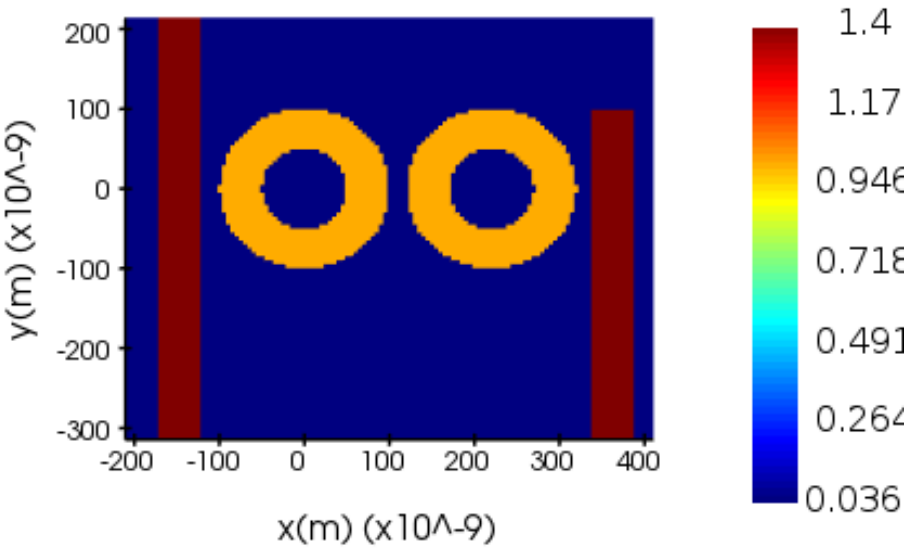


*Figure 6. 10 Refractive index profile of the structure*

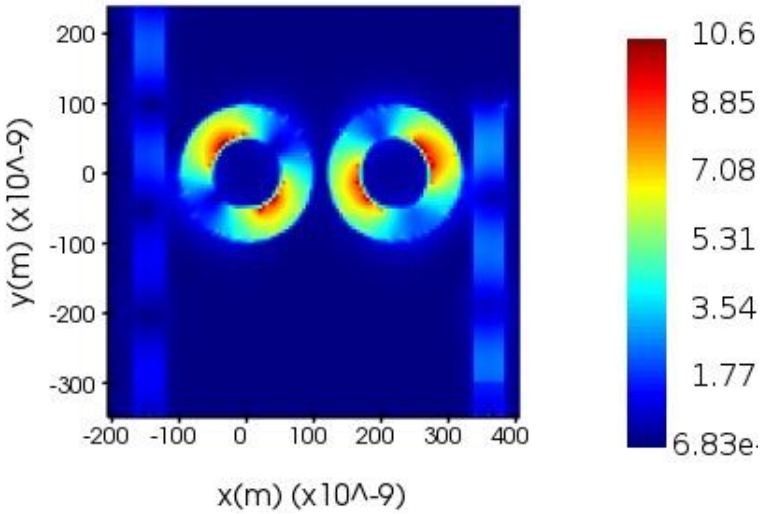


*Figure 6. 11 Electric field distribution when input source is disabled*

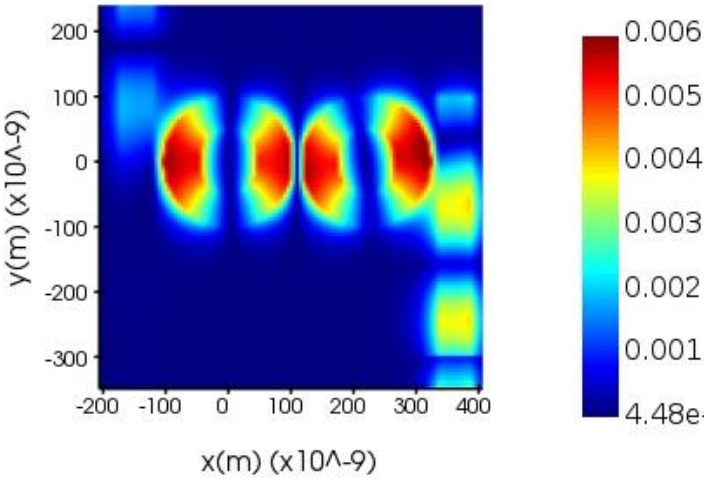


*Figure 6. 12 Magnetic field distribution when input source is disabled*

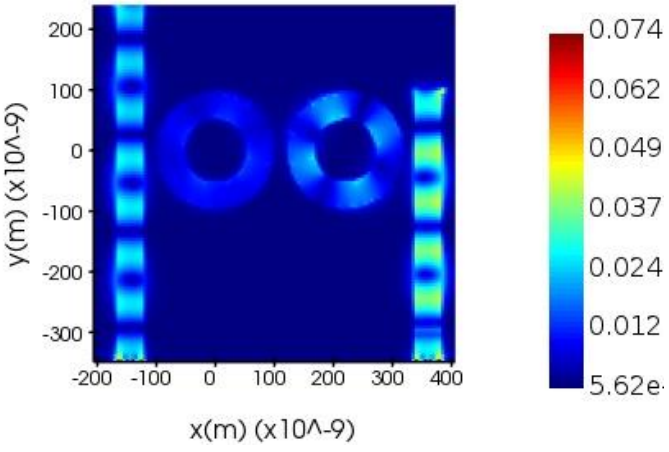


*Figure 6. 13 Power distribution when input source is disabled*

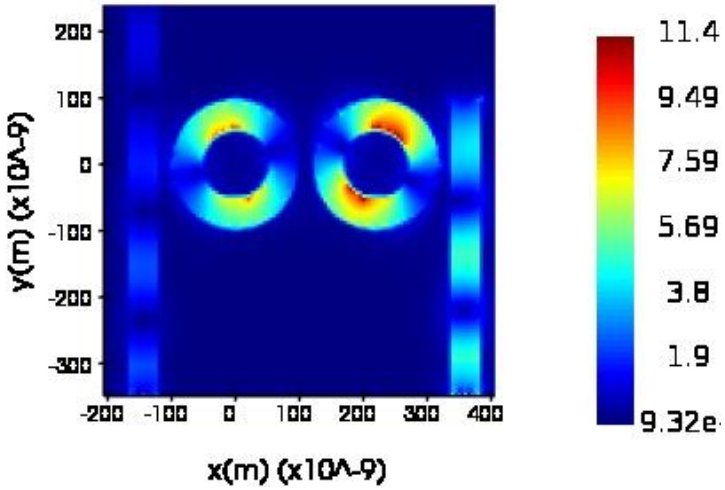


*Figure 6. 14 Electric field distribution when input source is enabled*

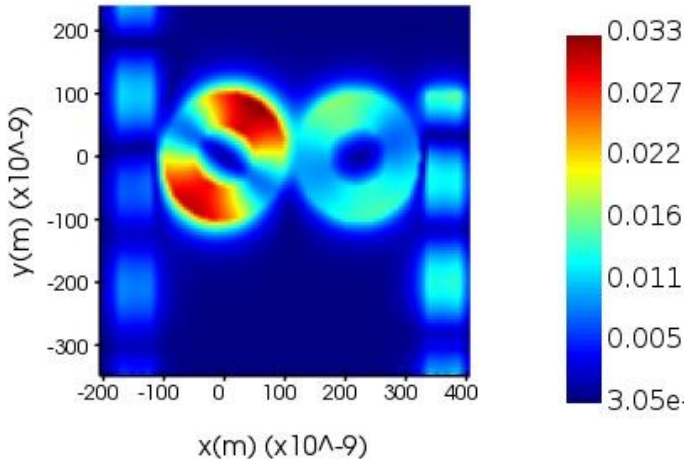


*Figure 6. 15 Magnetic field distribution when input source is disabled*

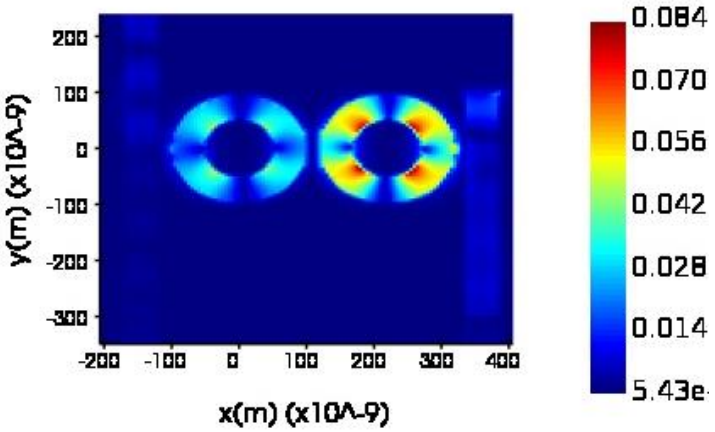


*Figure 6. 16 Power distribution when input source is disabled*

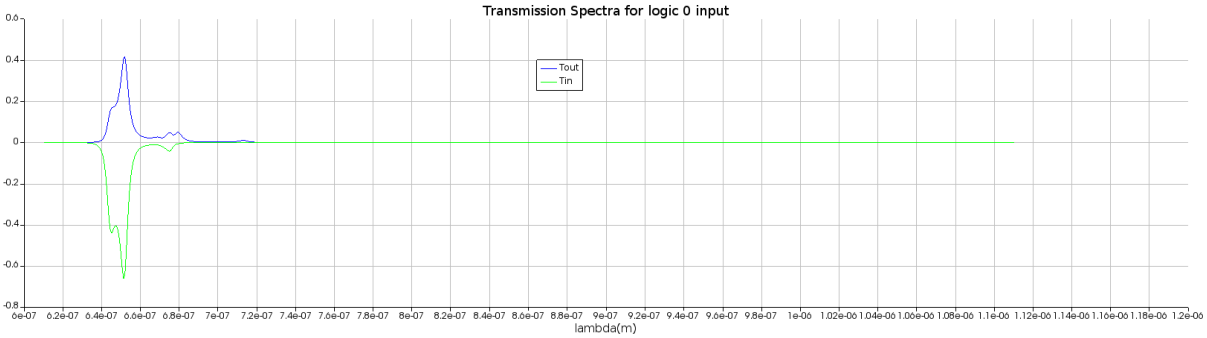


*Figure 6. 17 Transmission Spectrum at Output port when input is disabled*

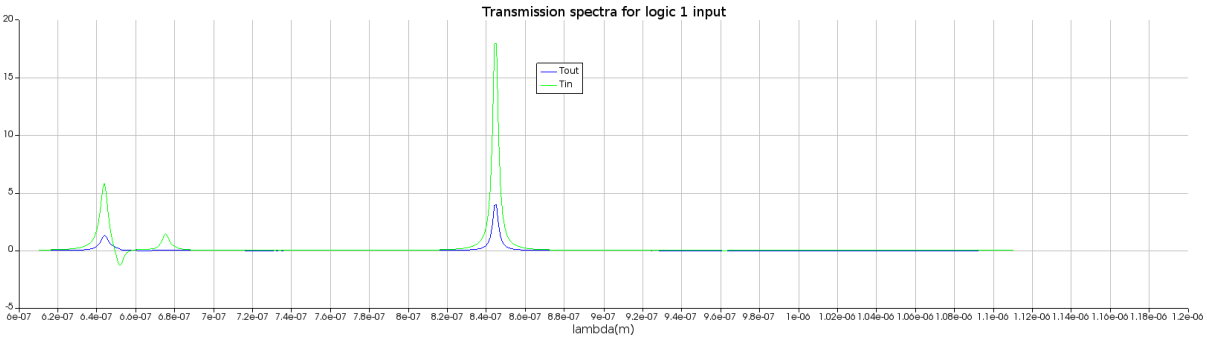


*Figure 6. 18 Transmission Spectrum at Output port when input is enabled*

# CHAPTER 7

# CONCLUSION AND FUTURE SCOPE

The theoretical aspects of employing surface plasmon polaritons in all-optical logic was studied. The basic performance of microring resonators were investigated in an aim to use it realize all optical logic. An SOI waveguide ring resonator was implemented to analyze the fundamental working of a microring resonator. It was designed for a Free Spectral Range of 25.6nm at 1550nm and an approximate Q factor of 2000. Ripples are observed in the transmission spectrum due to an early shutoff of simulation. Furthermore, an Ag-Air-Ag MIM waveguide ring resonator was used to realize NOT logic and the functionality was achieved with an acceptable threshold between ON and OFF states. An amplification in the ports were observed due to early shutoff of simulation. The method used for solving the Maxwell's in both the structures is Finite Difference Time Domain and the applied boundary condition is Perfectly Matched Layers (PML).

## Future Work

This work can be extended to realize all the basic gates and universal gates and further to basic logic modules like MUX, DEMUX, Flipflop, Half Adder, Full Adder etc. Also works should be done to improvise the waveguide structure in terms of materials, geometry and area footprint. Further the logic data can be encoded in a different parameter of the light like phase rather than intensity. Improvements needs to done in the cascadability of the structure since an MIM waveguide has a low propagation length.

# REFERENCES


[1] Ozbay E. Plasmonics: merging photonics and electronics at nanoscale dimensions. Science. 2006 Jan 13;311(5758):189-93. doi: 10.1126/science.1114849. PMID: 16410515.

[2] Minzioni, P. et al. "Roadmap on all-optical processing." *Journal of Optics* 21 (2019): 063001.

[3] Almeida VR, Barrios CA, Panepucci RR, Lipson M. All-optical control of light on a silicon chip. Nature. 2004 Oct 28;431(7012):1081-4. doi: 10.1038/nature02921. PMID: 15510144.

[4] Sanmukh Kaur and Rajinder-Singh Kaler, "Ultrahigh Speed Reconfigurable Logic Operations Based on Single Semiconductor Optical Amplifier," J. Opt. Soc. Korea 16, 13-16 (2012)

[5] S. Maksymov, "Optical switching and logic gates with hybrid plasmonic-photonic crystal nanobeam cavities," Phys. Lett. A 375(5), 918–921 (2011).

[6] Q. Xu and M. Lispon, "All-optical logic based on silicon micro-ring resonators," Opt. Express 15(3), 924–929 (2007).

[7] Wei, H., Wang, Z., Tian, X. et al. Cascaded logic gates in nanophotonic plasmon networks. Nat Commun 2, 387 (2011). https://doi.org/10.1038/ncomms1388

[8] Dolatabady and N. Granpayeh, "All optical logic gates based on two dimensional plasmonic waveguides with nanodisk resonators," J. Opt. Soc. Korea 16(4), 432–442 (2012).

[9] Y.-D. Wu, Y.-T. Hsueh, and T.-T. Shih, "Novel all-optical logic gates based on microring metal-insulator-metal plasmonic waveguides," in PIERS Proc., pp. 169–172 (2013).

[10] Fu Y, Hu X, Lu C, Yue S, Yang H, Gong Q. All-optical logic gates based on nanoscale plasmonic slot waveguides. Nano Lett. 2012 Nov 14;12(11):5784-90. doi: 10.1021/nl303095s. Epub 2012 Nov 2. PMID: 23116455.

[11] Najmeh Nozhat and Nosrat Granpayeh, "All-optical logic gates based on nonlinear plasmonic ring resonators," Appl. Opt. 54, 7944-7948 (2015)

[12] Saif H. Abdulnabi, Mohammed N. Abbas, "All-optical logic gates based on nanoring insulator–metal– insulator plasmonic waveguides at optical communications band," J. Nanophoton. 13(1), 016009 (2019), doi: 10.1117/1.JNP.13.016009.

[13] Fakhruldeen, Hassan Falah & Mansour, Tahreer. (2020). Design and Simulation of All-Optical Plasmonic Logic Gates Based on Nano-Ring Insulator-Metal-Insulator Waveguides. 29. 405-425. 10.26782/jmcms.2020.02.00015.

[14] S. A. Maier, *Plasmonics: fundamentals and applications*, Berlin Heideberg: Springer, 2007: 53.

[15] Bogaerts, W., De Heyn, P., Van Vaerenbergh, T., De Vos, K., Kumar Selvaraja, S., Claes, T., Dumon, P., Bienstman, P., Van Thourhout, D. and Baets, R. (2012), Silicon microring resonators. Laser & Photon. Rev., 6: 47-73. https://doi.org/10.1002/lpor.201100017

[16] Inan, U., & Marshall, R. (2011). Numerical Electromagnetics: The FDTD Method. Cambridge: Cambridge University Press. doi:10.1017/CBO9780511921353

[17] Bermúdez A., Hervella–Nieto L., Prieto A., Rodríguez R. (2008) Perfectly Matched Layers. In: Marburg S., Nolte B. (eds) Computational Acoustics of Noise Propagation in Fluids - Finite and Boundary Element Methods. Springer, Berlin, Heidelberg. https://doi.org/10.1007/978-3-540-77448-8_7